NASA TECHNICAL NOTE

NASA TN D-8519 c.1

NASA TN D-8519

RECENT ADVANCES IN AERODYNAMIC ENERGY CONCEPT FOR FLUTTER SUPPRESSION AND GUST ALLEVIATION USING ACTIVE CONTROLS

E. Nissim

Langley Research Center
Hampton, Va. 23665

NATIONAL AERONAUTICS AND SPACE ADMINISTRATION • WASHINGTON, D. C. • SEPTEMBER 1977

1. Report No. NASA TN D-8519	2. Government Accession No.
4. Title and Subtitle: RECENT ADVANCES IN AERODYNAMIC ENERGY CONCEPT FOR FLUTTER SUPPRESSION AND GUST ALLEVIATION USING ACTIVE CONTROLS	5. Report Date: September 1977
	6. Performing Organization Code
7. Author(s): E. Nissim	8. Performing Organization Report No. L-11707
	10. Work Unit No. 743-05-04-01
9. Performing Organization Name and Address: NASA Langley Research Center, Hampton, VA 23665	11. Contract or Grant No.
	13. Type of Report and Period Covered: Technical Note
12. Sponsoring Agency Name and Address: National Aeronautics and Space Administration, Washington, DC 20546	14. Sponsoring Agency Code

15. Supplementary Notes

NRC-NASA Senior Resident Research Associate; now at Technion-Israel Institute of Technology, Haifa, Israel.

16. Abstract

Control laws are derived, by using realizable transfer functions, which permit relaxation of the stability requirements of the aerodynamic energy concept. The resulting aerodynamic eigenvalues indicate that both the trailing-edge and the leading-edge—trailing-edge control systems can be made more effective. These control laws permit the introduction of aerodynamic damping and stiffness terms in accordance with the requirements of any specific system. Flutter suppression and gust-alleviation problems can now be treated by either a trailing-edge control system or by a leading-edge—trailing-edge control system by using the aerodynamic energy concept. Results are applicable to a wide class of aircraft operating at subsonic Mach numbers.

17. Key Words (Suggested by Author(s)): Flutter suppression Gust alleviation Active controls	18. Distribution Statement: Unclassified - Unlimited Subject Category 39

19. Security Classif. (of this report)	20. Security Classif. (of this page)	21. No. of Pages	22. Price*
Unclassified	Unclassified	66	$4.50

* For sale by the National Technical Information Service, Springfield, Virginia 22161

CONTENTS

RECENT ADVANCES IN AERODYNAMIC ENERGY CONCEPT FOR FLUTTER SUPPRESSION AND GUST ALLEVIATION USING ACTIVE CONTROLS

E. Nissim*
Langley Research Center

SUMMARY

Control laws are derived, by using realizable transfer functions, which permit relaxation of the stability requirements of the aerodynamic energy concept. The resulting aerodynamic eigenvalues indicate that both the trailing-edge and the leading-edge—trailing-edge control systems can be made more effective. These control laws permit the introduction of aerodynamic damping and stiffness terms in accordance with the requirements of any specific system. Flutter suppression and gust alleviation problems can now be treated by either a trailing-edge control system or by a leading-edge—trailing-edge control system by using the aerodynamic energy concept. Results are applicable to a wide class of aircraft operating at subsonic Mach numbers.

INTRODUCTION

Flutter suppression and gust-alleviation systems using active controls tend to be very sensitive to system changes caused by different flight conditions (flight speed, flight altitude, flight duration, and type of mission). The aerodynamic energy concept (ref. 1) was formulated in an attempt to define active control systems which do not exhibit such sensitivities to changing flight conditions. Although recent applications of the aerodynamic energy concept to specific problems of flutter suppression (refs. 2 and 3) and gust alleviation (ref. 3) yielded encouraging results, it was indicated that the derived control laws could be improved.

In the original development of the aerodynamic energy concept, idealized transfer functions were employed. These idealized transfer functions were difficult to realize and only approximate implementations could be made (ref. 2). In addition, the aerodynamic energy concept contained stringent requirements of a sufficient, but not necessary, condition for stability which effectively ruled out the trailing-edge (T.E.) control as a single stabilizing control system in favor of a combined leading-edge—trailing-edge control system.

The present work reviews the aerodynamic energy approach in light of the experience obtained since its original development and describes a way of relax-

---

*NRC-NASA Senior Resident Research Associate; now at Technion-Israel Institute of Technology, Haifa, Israel.

ing the stringent stability conditions and improves the derived control laws by using realizable transfer functions. Both trailing-edge and leading-edge—trailing-edge control systems are investigated.

SYMBOLS

a_L	leading-edge free parameter
a_T	trailing-edge free parameter
b	semichord length
C_{ij}	element i,j of control law matrix $[C]$
G_{ij}	element i,j of control law matrix $[G]$
g_i	structural damping coefficient in ith mode
h	bending displacement, positive in down direction
i	$= \sqrt{-1}$
k	reduced frequency, $\frac{\omega b}{V}$
M	Mach number
M_R	mass ratio, defined in equation (B9)
m	mass
n	number of degrees of freedom
P	energy dissipated by system per cycle
Q_h, Q_α	generalized aerodynamic force along h and α, respectively
R	transfer function, defined in equation (27)
r	number of activated control surfaces
s	wing semispan or reference length
t	time
V	flight speed
α	oscillatory angle of attack of wing, positive in nose-up direction
β, δ	leading-edge and trailing-edge control surface deflections, respectively, positive in down direction

ζ damping coefficient

λ eigenvalue of $[U]$

$\bar{\lambda}$ $= k^2\lambda$

λ_d equivalent λ for structural damping

ρ fluid density

ω oscillatory frequency

Matrices:

$[A_R], [A_I]$ real and imaginary parts of aerodynamic matrix $[A]$ (see eq. (1))

$[\bar{A}_R], [\bar{A}_I]$ real and imaginary parts of aerodynamic matrix $[\bar{A}]$ (see eq. (15))

$[B]$ inertia matrix

$[C]$ control law matrix

$[E]$ structural stiffness matrix

$\{F\}$ column matrix of forces

$[G]$ control law matrix

$[Q_R], [Q_I]$ real and imaginary parts, respectively, of energy eigenvector modal matrix

$\{q\}, \{\bar{q}\}$ complex response vectors

$\{q_o\}$ complex amplitude of response vector

$\{q_R\}, \{q_I\}$ real and imaginary parts of $\{q_o\}$

$[T]$ transfer function matrix

$[U]$ energy matrix

$[\lambda]$ diagonal matrix of eigenvalues of $[U]$

$\{\xi_R\}, \{\xi_I\}$ real and imaginary parts, respectively, of generalized energy coordinates

$\{\eta\}$ eigenvector of $[U]$

Subscripts:

c	control
I	imaginary part of a complex value
max	maximum
min	minimum
R	reference, also real part of a complex value
s	structural

Other notations:

$\lvert\ \rvert$	absolute value
$[\ ]^T$	transposed matrix
*	complex conjugate
$[\ ]$	row matrix
$\{\ \}$	column matrix

Dots over symbols denote derivatives with respect to time.

THE AERODYNAMIC ENERGY APPROACH

Basic Concept

An active control system on a lifting surface, such as a wing, actuates a control surface in response to oscillations of the wing in a manner which stabilizes the system. Because flutter instabilities originate from aerodynamic forces acting on the wing, the possibility arises of changing the aerodynamic forces through an appropriate activation of control surfaces. The aerodynamic energy concept was developed (ref. 1) to examine this possibility. The concept centers around the work P done by aerodynamic forces on their surroundings, per cycle of oscillation. A control surface activation is sought that leads to large and positive values of P, thereby energy dissipation and stability are insured.

Development of energy concept.- In this section, the energy concept is redeveloped (with details presented in appendix A) both to help the reader follow the present work and to show that the original derivation pertains only to mass-balanced control systems.

The n equations

$$\{F\} = -\omega^2\left[B + \pi\rho b^4 s(A_R + iA_I)\right]\{\bar{q}\} + [E]\{\bar{q}\} \tag{1}$$

represent the equations of motion of n structural modes with r activated controls, where at flutter

$$\{F\} = 0$$

and

ω frequency of oscillation

$[B]$ $n \times (n + r)$ mass matrix (n natural modes and r active controls)

$[A_R], [A_I]$ real and imaginary parts of aerodynamic matrix, respectively

$[E]$ stiffness matrix

ρ fluid density

s reference length

b reference semichord length

$\{\bar{q}\}$ response vector comprising n structural modes and r control modes, $\{\bar{q}\} = \begin{Bmatrix} q \\ q_c \end{Bmatrix}$

The matrices in equation (1) can be partitioned into square matrices ($n \times n$) relating to the structural modes (subscripted by s) and rectangular matrices ($n \times r$) relating to control surface couplings (subscripted by c).

After partitioning the matrices, equation (1) becomes

$$\{F\} = \left(-\omega^2\left[\left[B_s \vdots B_c\right] + \pi\rho b^4 s\left(\left[A_{R,s} \vdots A_{R,c}\right] + i\left[A_{I,s} \vdots A_{I,c}\right]\right)\right] + \left[E_s \vdots E_c\right]\right)\begin{Bmatrix} q \\ q_c \end{Bmatrix} \tag{2}$$

Assume a control law of the form

$$\{q_c\} = [T]\{q\} \tag{3}$$

where $[T]$ is a $r \times n$ matrix representing the transfer functions of the control law. Substituting equation (3) into equation (2) yields

$$\{F\} = \Big(-\omega^2\Big[[B_s] + [B_c][T] + \pi\rho b^4 s\Big([A_{R,s}] + [A_{R,c}][T] + i[A_{I,s}] + i[A_{I,c}][T]\Big)\Big] + [E_s] + [E_c][T]\Big)\{q\} \tag{4}$$

The matrix $[E_c]$ is considered to be zero since it is assumed that no elastic couplings exist between the structural modes and the control deflections. As shown in appendix A, the work P done by the system on its surrounding per cycle can be written as (eq. (A12))

$$P = \frac{\pi^2\rho b^4 s\omega^2}{2}\{q_R - iq_I\}\Bigg[-\Big([A_{I,s}] + [A_{I,s}]^T + [A_{I,c}][T] + [T^*]^T[A_{I,c}]^T\Big) + i\Bigg(\frac{[B_c][T] - [T^*]^T[B_c]^T}{\pi\rho b^4 s} + [A_{R,s}] - [A_{R,s}]^T + [A_{R,c}][T] - [T^*]^T[A_{R,c}]^T\Bigg)\Bigg]\{q_R + iq_I\} \tag{5}$$

where (from eq. (A6))

$$\{q\} = \{q_o\}e^{i\omega t} = \{q_R + iq_I\}e^{i\omega t} \tag{6}$$

The sign of P determines stability, and therefore, it is advantageous to convert equation (5) to a more convenient form. As shown in appendix A (eq. (A20)), P can be reduced to the form

$$P = \frac{1}{2}\pi^2\rho b^4\omega^2 s\Big(\{\xi_R\}[\lambda]\{\xi_R\} + \{\xi_I\}[\lambda]\{\xi_I\}\Big) \tag{7}$$

or

$$P = \frac{1}{2}\pi^2\rho b^4\omega^2 s\Big[\lambda_1\Big(\xi_{R,1}^2 + \xi_{I,1}^2\Big) + \lambda_2\Big(\xi_{R,2}^2 + \xi_{I,2}^2\Big) + \ldots + \lambda_n\Big(\xi_{R,n}^2 + \xi_{I,n}^2\Big)\Big] \tag{8}$$

where $[\lambda]$ is a diagonal matrix of the eigenvalues λ_i, necessarily real, of the Hermitian matrix (eq. (A14))

$$[U] = \left[-\left([A_{I,s}] + [A_{I,s}]^T + [A_{I,c}][T] + [T^*]^T [A_{I,c}]^T \right) + i\left([A_{R,s}] - [A_{R,s}]^T + [A_{R,c}][T] - [T^*]^T [A_{R,c}]^T + \frac{[B_c][T] - [T^*]^T [B_c]^T}{\pi \rho b^4 s} \right) \right] \tag{9}$$

and where the vectors $\{\xi_R\}$ and $\{\xi_I\}$ are defined by the transformation (eq. (A15))

$$\{q_o\} = [Q_R + iQ_I]\{\xi_R + i\xi_I\} \tag{10}$$

The matrix $[Q_R + iQ_I]$ is a square modal matrix of the principal eigenvectors.

Discussion of energy concept.- The work per cycle P done by the system on its surroundings has a direct bearing on the stability of the system. If P is positive, the system is dissipative, and therefore stable. If P is negative, the system is unstable because work is done by the surroundings on the system. Equation (8) shows that if all the eigenvalues λ_i of the system are positive, the system is stable regardless of the motions represented by the generalized energy coordinates ξ. If one or more of the λ eigenvalues is negative, the system is potentially unstable. Its ultimate stability is determined by the relative values of the terms ξ and λ. If the ξ values make the positive eigenvalues dominate the right-hand side of equation (8), the work P is positive and the system is stable. If, on the other hand, the ξ values make the negative terms dominate equation (8), P is negative and the system is unstable. Hence, the requirement for all λ's to be positive is a sufficient but not a necessary condition for stability.

For mass-balanced control surfaces $([B_c] = 0)$, the eigenvalues λ obtained from $[U]$ (eq. (9)) are dependent only on the aerodynamic properties of the system and the activated control law (matrix $[T]$). In the case of mass-balanced surfaces the eigenvalues are referred to as aerodynamic eigenvalues and are, in general, functions of the reduced frequency k and Mach number M. If mass unbalance is a fixed quantity in the system, the eigenvalues λ also depend on the fluid density ρ in addition to their dependence on k and M. In the present work, only mass-balanced systems are treated and therefore eigenvalues are obtained from the following $[U]$ matrix (eq. (A21))

$$[U] = \left[-\left([A_{I,s}] + [A_{I,s}]^T + [A_{I,c}][T] + [T^*]^T [A_{I,c}]^T \right) + i\left([A_{R,s}] - [A_{R,s}]^T + [A_{R,c}][T] - [T^*]^T [A_{R,c}]^T \right) \right] \tag{11}$$

Equation (11) shows how the transfer function matrix $[T]$ affects the matrix $[U]$ and therefore affects the aerodynamic eigenvalues.

Generalized Model

The energy approach has been formulated for a general n degree-of-freedom system. Therefore, the energy concept can be applied to any problem. The results in this report, however, are specific for the system considered since the generalized aerodynamic forces depend not only on the system geometry but also on its structural modal responses. If, however, the energy concept is applied to a two-dimensional strip, the aerodynamic matrices are independent of geometry and responses of the system. As a result, the aerodynamic eigenvalues are independent of any specific system and are only functions of k, M, and the transfer function matrix $[T]$. Therefore, if $[T]$ is defined in accordance with the relaxed energy concept, using a two-dimensional strip as a model, these $[T]$ values are applicable to any three-dimensional wing within the limitations of strip theory; thus, the model is generally applicable. In the present work, the two-dimensional strip model is adopted in much the same way as in the original derivation of the energy concept. Sketch (a) illustrates the system considered, and the arrows indicate positive displacements and rotations.

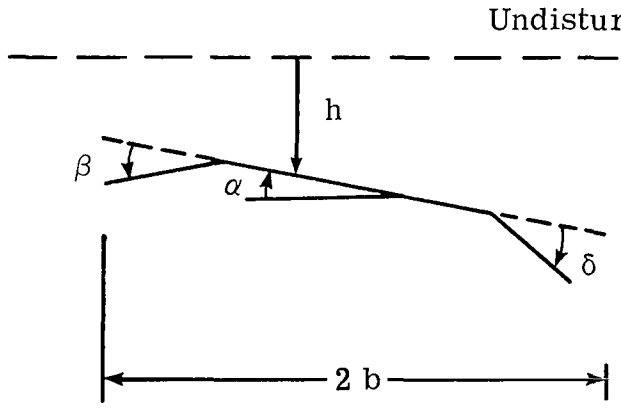

Sketch (a)

Relaxation of Energy Concept

The energy approach, in its original development, sought to determine the matrix $[T]$ to render all the aerodynamic eigenvalues large and positive. This requirement regarding the aerodynamic eigenvalues insures both the stability of the system (since P is always positive) and its insensitivity to various flight conditions (which manifest themselves in the form of changing values of λ and changing values of the system responses ξ). Assume that a relaxation is now introduced which permits some of the aerodynamic eigenvalues to be negative. Stability can be achieved under these conditions by modifying the responses of the system to render the responses associated with the positive eigenvalues to be the dominant ones. This latter requirement forms a necessary condition for stability but does not insure, in itself, the insensitivity of the resulting stabilized system to the various flight conditions. In order to insure that this relaxed stability requirement yields a system which shows only small sensitivities to the changing flight conditions

the absolute values of the negative aerodynamic eigenvalues must always be made much smaller than those eigenvalues associated with the dominant responses of the stabilized system. For the generalized two-dimensional model adopted in this work, two aerodynamic eigenvalues, λ_{min} and λ_{max}, are obtained. In the original derivation of the aerodynamic energy concept, λ_{min} was required to be positive and large. In the relaxed energy approach, λ_{min} is permitted to be negative provided

$$\lambda_{max} >> |\lambda_{min}| \qquad (\lambda_{min} < 0)$$

and provided that this inequality is maintained for all flight conditions. This relaxation is made possible by abandoning the sufficiency condition for stability in the original formulation while maintaining its insensitivity to changes in flight conditions. It should be stressed at this stage that the generalized two-dimensional flutter model adopted herein serves only to indicate, on the basis of the strip theory, whether energy is dissipated or absorbed by the partial span strip where the activated controls are installed. Therefore, to suppress flutter with a minimum number of activated partial span strips, enough energy should be dissipated in the activated strip to compensate for energy input by the nonactivated portions of the wing. Not only should λ_{min} be made positive but also λ_{min} might assume large (and positive) values. Since the dissipation of energy by the activated strip depends both on λ_{min} and on λ_{max}, the importance of λ_{max} should not be overlooked even when λ_{min} is positive and large. Considerable improvements in the potential performance of the activated control system may result, if changes in the control gains are permitted which lead to small degradations in λ_{min}, provided these degradations are accompanied by large increases in λ_{max}. It is therefore required to determine the optimum values of the transfer function matrix $[T]$ to lead to

$$\lambda_{min} = \text{Near maximum value (may be negative)}$$

$$\lambda_{max} >> |\lambda_{min}|$$

These two requirements regarding λ_{min} and λ_{max} are referred to in this work as the "relaxed energy requirements."

Formulation of a revised optimization procedure.- The optimization procedure used in the original development of the energy concept consisted of the following basic steps:

(1) Define the generalized aerodynamic forces Q_h and Q_α acting on a unit span of the two-dimensional strip and express them in the form

$$\begin{Bmatrix} Q_h \\ Q_\alpha \end{Bmatrix} = \pi\rho b^4\omega^2 \left[\left([A_{R,s}] + i[A_{I,s}] \right) \begin{Bmatrix} h/b \\ \alpha \end{Bmatrix} + \left([A_{R,c}] + i[A_{I,c}] \right) \begin{Bmatrix} \beta \\ \delta \end{Bmatrix} \right] \quad (12)$$

where all the matrices are of order 2 × 2.

(2) Assume a form for the matrix $[T]$ where $\begin{Bmatrix} \beta \\ \delta \end{Bmatrix} = [T] \begin{Bmatrix} h/b \\ \alpha \end{Bmatrix}$.

(3) For a given Mach number M and initial values for the gains in $[T]$, compute the numerical value of $[U]$ for a specific value of k.

(4) Compute the two eigenvalues resulting from $[U]$ and designate them as λ_{min} and λ_{max}.

(5) For a fixed value of M and $[T]$, repeat steps (1) to (4) for different values of k within the range $0.0128 \leq k \leq 19.5$ $(0.05 \leq 1/k \leq 78)$.

(6) Determine the area under the curve defined by the variation of λ_{min} with $1/k$.

(7) Optimize the gains in matrix $[T]$ to obtain a maximum area under the curve of λ_{min} as a function of $1/k$.

This seven-step procedure, which used the area under the curves of λ_{min} against $1/k$ as a target function, was found to be generally satisfactory. However, a plot of λ_{min} against $1/k$ and λ_{max} against $1/k$ for the unactivated system (fig. 1) shows that the very low frequency part of the curve contributes most to the target function. It is therefore possible that large improvements in the values of λ_{min} at intermediate frequencies may be completely "masked" during the optimization process if accompanied by very small degradations of λ_{min} at very low frequencies (high $1/k$ values).

A reexamination of the λ_{min} against $1/k$ behavior, undertaken in the present work, has led to the following two initial changes:

(a) The very large aerodynamic eigenvalues at the very low k range follow from the representation of the aerodynamic forces

$$\{F_A\} = \pi\rho b^4\omega^2 s \left([A_R] + i[A_I] \right) \{\bar{q}\} \quad (13)$$

The matrices $[A_R]$ and $[A_I]$ do not contain the true variation of the aerodynamic forces with k because of the ω^2 terms left outside the matrices. The frequency ω is not constant and varies with every mode of oscillation. A more rational representation of $\{F_A\}$, which maintains the full dependence of the aerodynamic matrices on k, can be expressed by

$$\{F_A\} = \pi\rho b^2 V^2 s\left(\left[\bar{A}_R\right] + i\left[\bar{A}_I\right]\right)\{\bar{q}\} \tag{14}$$

where V is the flight speed and

$$\left[\bar{A}_R\right] + i\left[\bar{A}_I\right] = k^2\left(\left[A_R\right] + i\left[A_I\right]\right) \tag{15}$$

Equation (14) leads to the following change in equation (8) (for $n = 2$):

$$P = \frac{1}{2}\pi^2\rho b^2 V^2 s\left[\bar{\lambda}_1\left(\xi_{R,1}^2 + \xi_{I,1}^2\right) + \bar{\lambda}_2\left(\xi_{R,2}^2 + \xi_{I,2}^2\right)\right] \tag{16}$$

where

$$\bar{\lambda}_i = k^2\lambda_i \tag{17}$$

Hence, for $k < 1$, the newly defined eigenvalues $\bar{\lambda}_i$ are smaller than the originally defined eigenvalues λ_i by a factor of k^2.

(b) The k range in the original derivation ($0.0128 \leqq k \leqq 19.5$) was unnecessarily wide. In the low k range, gust-alleviation problems generally occur around $k \approx 1/8$; in the high k range, the accuracy of the aerodynamic derivatives is questionable for values of $k > 3.5$. Therefore, the k range adopted was

$$\frac{1}{25} \leqq k \leqq 3.5$$

or

$$\frac{1}{3.5} \leqq \frac{1}{k} \leqq 25$$

The optimization algorithm used in the original development of the energy approach was found to be deficient in many respects. The algorithm used in the present work consists of a variation of Stewart adaptation (ref. 4) of the Davidon-Fletcher-Powell method (ref. 5). The variation introduced permits the different elements of the matrix $[T]$ to be constrained within preassigned limits without resorting to penalty functions and with excellent convergence characteristics.

In accordance with the relaxed energy concept there remains the problem of permitting small degradations in $\bar{\lambda}_{min}$ if accompanied by large increases in $\bar{\lambda}_{max}$. The initial approach was based on adding to the target function a weighted value of the area under the curve of $\bar{\lambda}_{max}$ against $1/k$. This

approach, although effective, leaves the value of the weight as an arbitrary parameter for the designer. However, as the present work progressed, the parameters which appreciably increase $\bar{\lambda}_{max}$ with relatively small degradations in $\bar{\lambda}_{min}$ have been identified, and the optimization procedure was modified in a manner which avoided weighting $\bar{\lambda}_{max}$. This point is discussed further in a later section of this paper.

Data and scope of optimization.- As in reference 1 and indicated in sketch (b), the two-dimensional strip has constant 20-percent-chord leading-edge (L.E.) and trailing-edge (T.E.) control surfaces. Similarly, a reference point for sensing the motion of the main surface was kept constant at 30 percent of the chord (measured from the leading edge). The gains associated with the control laws presented in this work refer therefore to the 30-percent chord point. These gains can be modified to accommodate a sensor located at a different point along the chord by employing a simple transformation matrix (ref. 1).

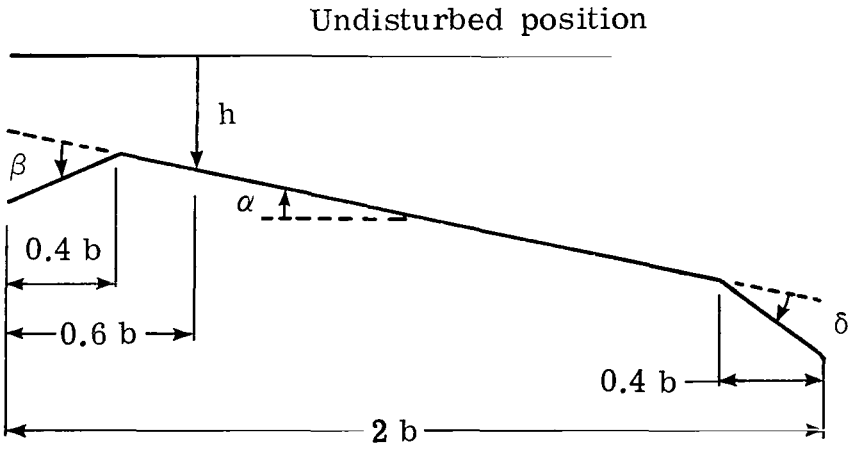

Sketch (b)

The investigation covers both a trailing-edge and a leading-edge—trailing-edge control system. Each of these control systems is driven by two different realizable transfer functions represented by the matrix $[T]$. The gains associated with each transfer function are optimized within a predetermined range of values by following the relaxed energy approach. Generalized control gains were tested for adequacy over wide ranges of reduced frequencies k, of subsonic Mach numbers M, and of maximum permissible gain values.

PRESENTATION AND DISCUSSION OF RESULTS

Results for the unactivated strip at various subsonic Mach numbers are presented first. These results form the basis for assessing any improvements introduced by the activated control systems. The results relating to each of the two transfer functions employed in this work are presented and discussed

separately. For each transfer function, a study is made of both the trailing-edge and the leading-edge—trailing-edge control systems.

Basic Nonactivated System

The variation of $\bar{\lambda}_{min}$ and $\bar{\lambda}_{max}$ with $1/k$ at different values of M, for a wing strip having no control surfaces (that is, $[T] = 0$) is shown in figure 2. The quantity $\bar{\lambda}_{min}$ is negative through most of the $1/k$ range, whereas $\bar{\lambda}_{max}$ is positive throughout the range of $1/k$. Furthermore, the negative $\bar{\lambda}_{min}$ values are of the same order of magnitude as $\bar{\lambda}_{max}$. Note also that the aerodynamic eigenvalues $\bar{\lambda}$ presented in figure 2 are greatly reduced in the high $1/k$ range when compared with the original eigenvalues λ (fig. 1).

Damping Type Transfer Function

The damping type transfer function (D.T.T.F.) is similar in form to the one used in reference 3; that is,

$$\begin{Bmatrix} \beta \\ \delta \end{Bmatrix} = \left([C] + \frac{b}{V}(i\omega)[G] \right) \begin{Bmatrix} h/b \\ \alpha \end{Bmatrix} \tag{18a}$$

or

$$\begin{Bmatrix} \beta \\ \delta \end{Bmatrix} = \left([C] + ik[G] \right) \begin{Bmatrix} h/b \\ \alpha \end{Bmatrix} \tag{18b}$$

where $[C]$ and $[G]$ are 2×2 constant matrices. Therefore, $[T]$ is given by

$$[T] = [C] + ik[G] \tag{19}$$

The control law represented by equations (18) differs from the one used in the original derivation of the energy approach (which used the term $i[G]$ instead of the $\frac{b}{V} i\omega[G]$ term). The implementation of the $\frac{b}{V} i\omega[G]$ term in equation (18a) is straightforward, whereas the implementation of the $i[G]$ term could only be achieved with great difficulties and in an approximate manner. The damping type transfer function was chosen for the relaxed energy approach because it is similar to the original control law and has been shown to be effective when applied to specific configurations (refs. 3 and 6) (by using the gains derived in ref. 1 for $[C]$ and $[G]$). The transfer function used in equation (19) is expressed in terms of ik in order to maintain the dependence of matrix $[U]$ (eq. (11)) on M and k only. Furthermore, equation (19)

represents the overall transfer function and implies that any actuator transfer functions should be compensated for to obtain the transfer function matrix.

On the basis of results obtained in reference 1, the aerodynamic eigenvalues are expected to increase if all the gains in matrix $[G]$ are increased by a constant factor. Hence, constraints are imposed on the G_{ij} gain values. The range chosen for $[G]$ is $-100 \leqq G_{ij} \leqq 100$. The effects of changing the nominal range are investigated in the present report. To reduce to a minimum the activation of the control surfaces at zero frequency, the following constraints are imposed on $[C]$:

$$C_{11} = C_{21} = C_{12} = 0$$

$$-2 \leqq C_{22} \leqq 2$$

The gain C_{22} is varied within a constrained range because of its large effects on the aerodynamic eigenvalues, as was shown in reference 1.

Results for trailing-edge control.- The trailing-edge control surface was first optimized at $M = 0.9$ on the basis of the curves for $\bar{\lambda}_{min}$ against $1/k$ by following the procedure described earlier in this work (with zero weight for $\bar{\lambda}_{max}$). The optimum gains obtained for $[C]$ and $[G]$ are

$$[C] = \begin{bmatrix} 0 & 0 \\ 0 & -1.76 \end{bmatrix}$$

$$[G] = \begin{bmatrix} 0 & 0 \\ 4.6 & 1.53 \end{bmatrix}$$

The resulting $\bar{\lambda}_{min}$ and $\bar{\lambda}_{max}$ variations with $1/k$ are shown in figure 3. Although the values of $\bar{\lambda}_{min}$ are improved over those with no control system (fig. 2), these improvements are accompanied by a substantial reduction in $\bar{\lambda}_{max}$ over most of the $1/k$ range, with the exception of improved values at the low end of the $1/k$ range. (Typically, at lower Mach numbers the values of $\bar{\lambda}_{min}$ are less than those shown in fig. 3.) Optimum values of $[G]$ are small compared with the wide range of variation permitted the G_{ij} gains; that is, $-100 \leqq G_{ij} \leqq 100$. It may be argued that although $\bar{\lambda}_{min}$ seems to be bounded and its values cannot be improved beyond a certain maximum level, $\bar{\lambda}_{max}$ might be increased without substantially degrading $\bar{\lambda}_{min}$ in accordance with the relaxed energy requirements. The incorporation of the weighted area of $\bar{\lambda}_{max}$ against $1/k$ into the target function (in addition to the $\bar{\lambda}_{min}$) shows that both G_{21} and G_{22} are positive and increase monotonically with the increase in weight associated with $\bar{\lambda}_{max}$. Consequently, an appropriate weight could be assigned to $\bar{\lambda}_{max}$ which causes the larger term (G_{21}) to reach

the constraint. However, a simpler method is to assign G_{21} the value at the constraint and optimize for $\bar{\lambda}_{min}$ only. By following this procedure the optimized gains for $[C]$ and $[G]$ obtained at $M = 0.9$ are

$$[C] = \begin{bmatrix} 0 & 0 \\ 0 & 0.46 \end{bmatrix}$$

$$[G] = \begin{bmatrix} 0 & 0 \\ 100 & 79 \end{bmatrix}$$

The variations of $\bar{\lambda}_{min}$ and $\bar{\lambda}_{max}$ with $1/k$ are shown in figure 4. By comparison with figure 2 (no controls), the quantity $\bar{\lambda}_{min}$ shows improvement over most of the $1/k$ range. In comparison with figure 3, the values of $\bar{\lambda}_{min}$ in figure 4 are mostly negative and degraded. The values of $\bar{\lambda}_{max}$ in figure 4, however, are greatly improved over those in figures 2 and 3 especially at low values of $1/k$. The values of $\bar{\lambda}_{min}$ are much smaller than those of $\bar{\lambda}_{max}$ in accordance with the objectives set by the relaxed energy approach.

Effect of variation of optimization range of G_{ij}: The results in figures 3 and 4 relate to a G_{ij} range of 100. Computations made for smaller ranges of G_{ij} show that the value of C_{22} becomes increasingly important as the G_{ij} range is reduced. At the limit, when all the G_{ij} terms are set to zero, the C_{22} term provides the only means for improving the eigenvalues. (When the G_{ij} terms are large, C_{22} can be ignored.) Hence, in an attempt to reach optimized control values that do not exhibit sensitivities to the optimization range of G_{ij}, except for a constant factor common to all the G_{ij} terms, C_{22} was assigned a value of $C_{22} = -1.86$. This value was obtained by optimizing the control gains with zero G_{ij} gains. Reoptimizing with $C_{22} = -1.86$ and $G_{21} = 100$ resulted in the following transfer function:

$$[C] = \begin{bmatrix} 0 & 0 \\ 0 & -1.86 \end{bmatrix}$$

$$[G] = \begin{bmatrix} 0 & 0 \\ 100 & 80 \end{bmatrix}$$

Regardless of the value of the G_{ij} constraint, the ratio of G_{21}/G_{22} remains essentially constant. Therefore, the following form of the optimized transfer function (eq. (19)) is suggested:

$$[T] = \begin{bmatrix} 0 & 0 \\ 0 & -1.86 \end{bmatrix} + a_T(ik) \begin{bmatrix} 0 & 0 \\ 100 & 80 \end{bmatrix} \tag{20}$$

The free parameter a_T permits the variation of $\bar{\lambda}_{max}$ while keeping the ratio of G_{21}/G_{22} a constant. Figure 5 shows a comparison made at $M = 0.9$ between the curves of $\bar{\lambda}_{min}$ against $1/k$ obtained by optimizing the gains of $[T]$ for different maximum values of G_{21} (fig. 5(a)) and the curves obtained by using equation (20) with values of a_T chosen to obtain the same maximum values for G_{21} (fig. 5(b)). The values of $\bar{\lambda}_{min}$ for the low $1/k$ range are not shown in figure 5 in order to scale the ordinate to yield a good resolution among the different curves. (A similar representation, which will be adopted in many of the figures, has no reflection on the k range for which the optimization has been performed.) The differences between the $\bar{\lambda}_{min}$ curves in figures 5(a) and 5(b) are not significant in view of the large similar values of $\bar{\lambda}_{max}$ in figures 6(a) and 6(b). These results justify the form of the transfer function in equation (20).

Mach number effects: The effect of changing the flight Mach number on $\bar{\lambda}_{min}$ is shown in figure 7 for $G_{21} = 100$ and $C_{22} = -1.86$. Figure 7(a) is obtained by optimizing the gains at the different Mach numbers, whereas figure 7(b) shows the values obtained by using equation (20) with $a_T = 1$. Once again the differences between the $\bar{\lambda}_{min}$ curves in figure 7 are not significant in view of the similar and large values of $\bar{\lambda}_{max}$ shown in figure 8.

Results for leading-edge—trailing-edge control system.- An identical procedure to the one discussed in the trailing-edge system has been adopted for the leading-edge—trailing-edge control system in an attempt to optimize $\bar{\lambda}_{min}$ and take account of $\bar{\lambda}_{max}$. Here again C_{22} is assigned a value of -1.86 and $G_{21,max}$ is assigned the nominal value of 100. The following optimized gains are obtained for the leading-edge—trailing-edge system:

$$[C] = \begin{bmatrix} 0 & 0 \\ 0 & -1.86 \end{bmatrix}$$

$$[G] = \begin{bmatrix} -100 & 100 \\ 100 & 80 \end{bmatrix}$$

The variation of $\bar{\lambda}_{min}$ and $\bar{\lambda}_{max}$ with $1/k$, at $M = 0.9$, is shown in figure 9. The large improvements in $\bar{\lambda}_{min}$, as compared with the trailing-edge system (fig. 7), can be observed in figure 9(a) for all values of $1/k$. The values of $\bar{\lambda}_{max}$ in figure 9(b) are essentially the same as those obtained for the trailing-edge system (fig. 8). This situation implies that the optimum leading-edge control gains essentially affect $\bar{\lambda}_{min}$ with negligible effects on $\bar{\lambda}_{max}$. On the other hand, optimum trailing-edge control gains mainly influence $\bar{\lambda}_{max}$ and have little effect on $\bar{\lambda}_{min}$.

Effect of variation of the optimization range of G_{ij}: Optimum control laws were derived for different values of optimization ranges by using a procedure identical to that used for the trailing-edge control system. The results obtained for $\bar{\lambda}_{min}$ are shown in figure 10(a) and are compared in figure 10(b) with the values of $\bar{\lambda}_{min}$ obtained by using the suggested values for $[C]$ and $[G]$. (The suggested values of $[G]$ are scaled to span the appropriate G_{ij} range.) A similar comparison is made in figure 11 regarding the variation of $\bar{\lambda}_{max}$. The agreement obtained in figures 10 and 11 together with the localization of the leading-edge effects to the values of $\bar{\lambda}_{min}$ lead to the following more general formulation of the control gains:

$$[T] = \begin{bmatrix} 0 & 0 \\ 0 & -1.86 \end{bmatrix} + ik \begin{bmatrix} a_L & \\ & a_T \end{bmatrix} \begin{bmatrix} -100 & 100 \\ 100 & 80 \end{bmatrix} \tag{21}$$

where a_L and a_T are positive free parameters. The value of a_L essentially determines the levels of $\bar{\lambda}_{min}$ whereas the value of a_T essentially determines the levels of $\bar{\lambda}_{max}$. If the value of $a_L = 0$ is substituted in equation (21), the resulting matrix $[T]$ is identical to the one pertaining to the trailing-edge control, as presented in equation (20). Hence, equation (21), together with the parameters a_L and a_T, is applicable to both trailing-edge and leading-edge—trailing-edge control systems.

Mach number effects: The effects of Mach number on the variation of $\bar{\lambda}_{min}$ with $1/k$ for $G_{21} = 100$ and $C_{22} = -1.86$ are shown in figure 12. Figure 12(a) is obtained by optimizing the gains at the different Mach numbers, whereas figure 12(b) shows the values of $\bar{\lambda}_{min}$ as a function of $1/k$ as obtained by using equation (21) with $a_L = a_T = 1$. As can be seen, the figures are almost identical. Similar results are obtained for the accompanying variation of $\bar{\lambda}_{max}$ with $1/k$ shown in figures 13(a) and 13(b). Figures 14 and 15 are identical to figures 12 and 13 except that they show the variation of the different $\bar{\lambda}$ values at the low end of the $1/k$ range. A deterioration in the values of $\bar{\lambda}_{min}$ and $\bar{\lambda}_{max}$ occurs at low $1/k$ values as the Mach numbers are reduced and especially when $M = 0$. However, since the results pertaining to $M = 0$ are meaningless for practical applications and since the reduced values of $\bar{\lambda}_{min}$ at the high $1/k$ range are shown in the following section to be relatively less important, no attempt is made to improve the $\bar{\lambda}_{min}$ behavior at low $1/k$ values at the expense of some degradation at the higher range of $1/k$.

Effect of structural damping.- To understand the meaning of a specific value of an aerodynamic eigenvalue, it is convenient to express the structural damping in terms of an equivalent aerodynamic eigenvalue λ_d (the full development of the expression for λ_d is given in appendix B). The structural damping force acting on the ith mode is given by equation (B1) as

$$F_{d,i} = ig_i\omega_{n,i}^2 b_R m_i q_i \tag{22}$$

where g_i is the structural damping coefficient, $\omega_{n,i}$ is the natural frequency, m_i is the generalized mass, q_i is the nondimensional generalized modal response, and b_R is a reference wing semichord. The subscript i relates the parameters to the ith generalized mode. It can be shown (see appendix B for details) that the work W done per cycle by the force $F_{d,i}$ is given by equation (B7) as

$$W = \frac{1}{2}\pi^2\rho b_c^2 V^2 s_c \lambda_{d,i} q_{o,i}^2 = \pi g_i \omega_{n,i}^2 b_R^2 m_i q_{o,i}^2$$

where b_c is the semichord at the control-surface midspan region and s_c is the control-surface span. This equation yields (eq. (B10))

$$\lambda_{d,i} = 2g_i\left(\frac{b_R}{b_c}\right)^4 \frac{s}{s_c} k_{n,c,i}^2 M_{R,i} \tag{23}$$

where $k_{n,c,i}$ is defined by equation (B11) as

$$k_{n,c,i} = \frac{\omega_{n,i} b_c}{V} \tag{24}$$

For a two-dimensional strip, $s = s_s$, $b_R = b_c$, and equation (23) reduces to

$$\lambda_{d,i} = 2g_i k_{n,c,i}^2 M_{R,i} \tag{25}$$

Equation (25) shows that a fixed value of structural damping converts to an increasingly larger equivalent aerodynamic eigenvalue as the reduced frequency $k_{n,c,i}$ is increased. Therefore, a value of $\bar{\lambda}_{min} = -1$, for example, at $k_{n,c,i} = 0.1$ is equivalent to a structural damping coefficient 1225 times larger than the one obtained if the same value of $\bar{\lambda}_{min} = -1$ is obtained at $k_n = 3.5$ $\left(1225 = \left(\frac{3.5}{0.1}\right)^2\right)$. This example illustrates the relative importance of the aerodynamic eigenvalues in different regions of the k range and stresses the importance of the low k range over the higher k range.

Summarizing remarks regarding damping type transfer function.- The relaxed energy approach, when used in conjunction with the damping type transfer function, yields fixed control gain ratios for both the trailing-edge and the leading-edge—trailing-edge control systems, which are effective over a

wide range of reduced frequency k and of control gain factors a_L and a_T. It is shown that although the trailing-edge control system shows improvements in the $\bar{\lambda}_{min}$ values, these improvements are bounded and cannot be improved beyond a certain maximum value. The values for $\bar{\lambda}_{max}$, however, are shown to be unbounded and increase continuously with a_T. The leading-edge—trailing-edge system shows unbounded improvements over a wide range of k values for both $\bar{\lambda}_{min}$ and $\bar{\lambda}_{max}$. The gain a_L essentially affects the $\bar{\lambda}_{min}$ values with only little effect on $\bar{\lambda}_{max}$, whereas the gain a_T essentially affects the values of $\bar{\lambda}_{max}$ with little effect on $\bar{\lambda}_{min}$. This unbounded behavior is typical of a dynamic system to which damping is added. For this reason the $[G]$ matrix is regarded essentially as a damping matrix introduced through the activation of the control surfaces.

Two major criticisms can be made regarding the damping type transfer function:

(1) The damping type transfer function does not permit the introduction of damping into the system over a limited range of k values. Instead, damping is introduced over an uncontrolled range of k values. Hence, a penalty may be paid in terms of unnecessary control-surface activity.

(2) The term $ik[G]$ that appears in the damping type transfer function (eq. (19)) increases indefinitely with k. As a result, stability problems may develop at very high k values beyond the range investigated in this work.

In addition to these criticisms, the relaxed energy approach does not rule out the use of stiffness terms in order to change the response of the system to increase the response associated with $\bar{\lambda}_{max}$. The damping type transfer function permits the introduction of aerodynamic stiffness terms through the matrix $[C]$. This situation is inconvenient and very limiting since the matrix $[C]$ has a direct effect on the static behavior of the system.

These points lead to the formulation of the localized damping type transfer function which is presented later.

Localized Damping Type Transfer Function

The following transfer function is a direct outgrowth of the criticism of the damping type transfer function:

$$\begin{Bmatrix} \beta \\ \delta \end{Bmatrix} = \left([C] + \frac{(ik)^2}{(ik)^2 + 2\zeta k_n (ik) + k_n^2} [G] \right) \begin{Bmatrix} h/b \\ \alpha \end{Bmatrix} \tag{26}$$

where both ζ and k_n are constants. Direct comparison between equations (26) and (18) shows that the term ik in the damping type transfer function has been replaced by the term $(ik)^2/[(ik)^2 + 2\zeta k_n(ik) + k_n^2]$. It is appropriate, therefore, to investigate the properties of this term and determine how it compares with the ik term.

Variation with k of localized damping type transfer function.- The variation with k of the localized damping type transfer function (L.D.T.T.F.) is essentially embedded in the term (see eq. (26))

$$R = \frac{(ik)^2}{(ik)^2 + 2\zeta k_n(ik) + k_n^2} \tag{27}$$

Defining X as

$$X = \frac{k}{k_n} \tag{28}$$

and substituting in equation (27) yields

$$R = \frac{-X^2}{-X^2 + 2i\zeta X + 1} \tag{29}$$

The denominator in equation (27) is identical in form to a transfer function representing a second order system with damping ζ and natural frequency k_n. Figure 16 shows the variation of the real and imaginary parts of R as a function of X and ζ. It can be seen that $R = 0$ when $k = 0$ and $R \to 1$ when $k \to \infty$. The imaginary part of R is always positive. For small values of ζ, very large values of R_I (that is, the imaginary part of R) are obtained, with a maximum value obtained around $k = k_n$. In addition, the variation of R_I with k is very rapid for small values of ζ. As the value of ζ is increased, R_I becomes smaller and its maximum values occur for $k > k_n$. In addition, the increased value of ζ reduces the variation of R_I with k. If R_I is associated with positive damping, then positive stiffness values are associated with positive values of R_R (that is, the real part of R) and negative stiffness values are associated with negative values of R_R. (Strictly speaking, some symmetrical aerodynamic stiffness terms may be introduced through formal multiplication of the aerodynamic forces and $[T]$. However, these terms appear to be small.) Therefore, the quadrature term ik can be locally simulated by R over a range of frequencies determined by both ζ and k_n. In addition, stiffness terms are introduced as R varies with k. These stiffness terms clearly vanish when $k = 0$ and therefore do not affect the static behavior of the system. A transfer function of the type $ik/(ik + a)$, where a is a real number, could also simulate the quadrature term ik, however, with reduced effectiveness and reduced control regarding "localization" of damping.

Remarks on localized damping type transfer function.- Because of the results obtained for the damping type transfer function and the similarities between the two transfer functions, the following values have been adopted for the localized damping type transfer function:

(1) C_{22} is assigned the value of -1.86 (derived for zero G_{ij} gains and therefore also applicable to the localized damping type transfer function) to maintain the effectiveness of the system for small values of matrix $[G]$. (All other C_{ij} values are maintained at zero.)

(2) A nominal optimization range for the G_{ij} elements is chosen as $-4 \leqq G_{ij} \leqq 4$. The smaller range for G_{ij} was chosen to yield approximately the same peak values for $\bar{\lambda}$ as obtained for the damping type transfer function at the low and intermediate ranges of k values.

Results for trailing-edge control system.- The trailing-edge control system is first optimized at $M = 0.9$, G_{ij} being constrained within the nominal range, and with $k_n = 0.2$ and $\zeta = 0.5$. Variation of these values is subsequently investigated.

Initial optimum values obtained for the matrix $[G]$ showed behavior identical to that of the damping type transfer function; that is, a deterioration in $\bar{\lambda}_{max}$ was obtained, and the resulting G_{ij} gains were very small in comparison with the span of the nominal G_{ij} range. By following an identical type of investigation as in the damping type transfer function case, an identical conclusion was drawn, that is, that optimization must be performed after assigning G_{21} the maximum positive value of its range. The results for the nominal range yield the following gains:

$$[C] = \begin{bmatrix} 0 & 0 \\ 0 & -1.86 \end{bmatrix}$$

$$[G] = \begin{bmatrix} 0 & 0 \\ 4 & 2.8 \end{bmatrix}$$

Figure 17 shows the resulting variation of $\bar{\lambda}_{min}$ and $\bar{\lambda}_{max}$ with $1/k$. Both $\bar{\lambda}_{min}$ and $\bar{\lambda}_{max}$ are positive throughout the $1/k$ range and $\bar{\lambda}_{max}$ shows "peaking" behavior at k_n (that is, $1/k = 1/0.2 = 5$). Figure 18 shows the variation of $\bar{\lambda}_{min}$ and $\bar{\lambda}_{max}$ with $1/k$ at different Mach numbers obtained by using these gains. Figure 18(a) shows a slight deterioration in $\bar{\lambda}_{min}$ as the Mach number is reduced and shows no signs of peaking at k_n. Figure 18(b) shows that the peaking characteristic of $\bar{\lambda}_{max}$ exists at all values of M. Figure 19 shows the variation of $\bar{\lambda}_{min}$ and $\bar{\lambda}_{max}$ with $1/k$ at $M = 0.9$ obtained by using these gains and scaling the $[G]$ matrix by various constant factors. The results show increased $\bar{\lambda}_{max}$ values throughout the range for most of the scaled gains of the $[G]$ matrix. A small variation in $\bar{\lambda}_{min}$ can be seen in figure 19(a), especially for the case where these values of $[G]$ are all multiplied by 2. Figure 20 shows the variation of $\bar{\lambda}_{min}$ and $\bar{\lambda}_{max}$ with ζ. The effect of varying ζ is seen to be similar to the effect of scaling $[G]$ (fig. 19), with the exception that the $\bar{\lambda}_{max}$ peaks become narrower as ζ is reduced and the dips which follow the peaks become more accentuated. Figure 21 shows the variation of $\bar{\lambda}_{min}$ and $\bar{\lambda}_{max}$ with $1/k$

at $M = 0.9$ for different values of k_n. The large improvements in $\bar{\lambda}_{max}$ are immediately apparent over a wide range of k values. The values of $\bar{\lambda}_{min}$, however, show a negative region for the value of $k_n = 0.1$. Comparison with the curve for the unactivated system (fig. 2) shows that around $k = 0.3$ $\left(\frac{1}{k} = 3.5\right)$, where $\bar{\lambda}_{min}$ is smaller, the degradation in $\bar{\lambda}_{min}$ is very small.

The following generalized control law is therefore suggested for the trailing-edge system:

$$\begin{Bmatrix} \beta \\ \delta \end{Bmatrix} = \left(\begin{bmatrix} 0 & 0 \\ 0 & -1.86 \end{bmatrix} + \frac{a_T(ik)^2}{(ik)^2 + 2i\zeta k_n k + k_n^2} \begin{bmatrix} 0 & 0 \\ 4 & 2.8 \end{bmatrix} \right) \begin{Bmatrix} h/b \\ \alpha \end{Bmatrix} \tag{30}$$

where a_T, ζ, and k_n are left as free parameters which determine the amount of damping introduced, the distribution as a function of k, and the location of the peak along the k-axis.

Results for leading-edge—trailing-edge control system.- The following optimum gains are obtained for the leading-edge—trailing-edge control system at $M = 0.9$ by using the nominal range for the G_{ij} gains (with $k_n = 0.2$ and $\zeta = 0.5$):

$$[C] = \begin{bmatrix} 0 & 0 \\ 0 & -1.86 \end{bmatrix}$$

$$[G] = \begin{bmatrix} -4 & 4 \\ 4 & 2.8 \end{bmatrix}$$

The resulting variation of $\bar{\lambda}_{min}$ and $\bar{\lambda}_{max}$ with $1/k$ is shown in figure 22. The variation of $\bar{\lambda}_{max}$ with $1/k$ is identical to that obtained for the trailing-edge control system (fig. 17) and implies that the leading-edge control gains have little or no effect on $\bar{\lambda}_{max}$. It has been shown that the trailing-edge control gains associated with $[G]$ have only a small effect on $\bar{\lambda}_{min}$. Therefore, the large values of $\bar{\lambda}_{min}$ shown in figure 22(a) are essentially due to the leading-edge control gains. The variation of $\bar{\lambda}_{min}$ and $\bar{\lambda}_{max}$ with Mach number, using these control gains, is shown in figure 23. Once again, $\bar{\lambda}_{max}$ remains essentially the same as that for the trailing-edge system whereas $\bar{\lambda}_{min}$ is greatly improved and shows large peaks at $k = k_n = 0.2$ (or $1/k = 5$).

The variation of the aerodynamic eigenvalues with the scaling factor of the matrix $[G]$ is shown in figure 24. Both $\bar{\lambda}_{min}$ and $\bar{\lambda}_{max}$ increase with the scaling factor over most of the range; this result implies that both $\bar{\lambda}_{min}$

and $\bar{\lambda}_{max}$ are unbounded in the leading-edge—trailing-edge system. The unbounded characteristic of the eigenvalues is observed once again in figure 25 where the value of ζ is varied. The peaks of $\bar{\lambda}_{max}$ in figure 25 are essentially located at $k = k_n$ whereas $\bar{\lambda}_{min}$ shows a peak at this location only for small values of ζ. As the value of ζ increased, the peaks move toward lower values of $1/k$. A study of the peak values in conjunction with R (fig. 16) indicates that the $\bar{\lambda}_{max}$ peaks occur at $R_R = 0$, or $k = k_n$. On the other hand, the $\bar{\lambda}_{min}$ peaks occur at the value of k which yields the largest response in quadrature R_I. Figure 16 shows that as ζ increases, $R_{I,max}$ is located along curves for which $k > k_n$. Therefore, if it is desired to maximize simultaneously $\bar{\lambda}_{min}$ and $\bar{\lambda}_{max}$ at a given value of k, the leading-edge control should be given a similar transfer function but with a smaller value of k_n. The effect of k_n on the aerodynamic eigenvalues is shown in figure 26. The results conform with the foregoing discussion. On the basis of these results, the following generalized control law is suggested:

$$\begin{Bmatrix} \beta \\ \delta \end{Bmatrix} = \left(\begin{bmatrix} 0 & 0 \\ 0 & -1.86 \end{bmatrix} + \begin{bmatrix} \dfrac{a_L(ik)^2}{(ik)^2 + 2\zeta_L k_{n,L}(ik) + k_{n,L}^2} & 0 \\ 0 & \dfrac{a_T(ik)^2}{(ik)^2 + 2\zeta_T k_{n,T}(ik) + k_{n,T}^2} \end{bmatrix} \begin{bmatrix} -4 & 4 \\ 4 & 2.8 \end{bmatrix} \right) \begin{Bmatrix} h/b \\ \alpha \end{Bmatrix} \tag{31}$$

where the subscript L refers to the leading-edge control and the subscript T refers to the trailing-edge controls. The six free parameters allow the amplitude of the different λ distributions, the width of the distributions, and their peak locations to be selected. If $a_L = 0$, equation (31) reduces to the trailing-edge control law given by equation (30).

Summarizing remarks regarding localized damping type transfer function.- The localized damping type transfer function is shown to have basically the same characteristics as the damping type transfer function regarding its effects on the values of $\bar{\lambda}_{min}$ and $\bar{\lambda}_{max}$, but within a localized range of k values. The deteriorating effects on $\bar{\lambda}_{min}$ shown by the damping type transfer function at high k values have either been eliminated or greatly reduced. Further improvement in $\bar{\lambda}_{min}$ for high k values can be obtained by means of the free parameters left in the generalized control law (eq. (31)). In addition, it can be shown that at sufficiently high values of k, the aerodynamic eigenvalues are proportional to k, that is, $\bar{\lambda} \propto k$, whereas the equivalent aerodynamic eigenvalue λ_d for the structural damping behaves as $\lambda_d \propto k^2$. Therefore, at sufficiently high frequencies, λ_d is dominant and the system is always stable (not the case for the D.T.T.F. where $\bar{\lambda} \propto k^2$). Since the values of $\bar{\lambda}_{min}$ at the highest value of k considered (=3.5) were seldom negative and assumed relatively small values, no special reference to this region was made during the discussion of the results. Finally, the free parameters left in the generalized control law, together with the stiffness properties exhibited by the localized damping type transfer function, make it

possible to tailor fit the results obtained herein to any specific system without exposing it to sensitivity hazards.

Sensitivity Test for the Gains

Sensitivity tests were conducted on the C_{ij} and G_{ij} gains for the two transfer functions and the two control systems investigated in this work. All the G_{ij} terms were found to be important (either for $\bar{\lambda}_{min}$ or for $\bar{\lambda}_{max}$), and no sudden deteriorations were observed with small to moderate parametric changes. Figure 27 is an illustrative example in which the value of G_{22}, using a trailing-edge system with localized damping type transfer function, is varied at $M = 0.9$. Both $\bar{\lambda}$ values are relatively insensitive to small changes in G_{22}. Finally, the gains obtained by the relaxed energy approach are different only in magnitude but not in sign as compared with those obtained in reference 1.

SIMPLIFIED CONTROL LAWS

The suggested generalized form of the damping type transfer function is given by equation (21) as

$$[T] = \begin{bmatrix} 0 & 0 \\ 0 & -1.86 \end{bmatrix} + ik \begin{bmatrix} a_L & \\ & a_T \end{bmatrix} \begin{bmatrix} -100 & 100 \\ 100 & 80 \end{bmatrix}$$

Equation (21) can be simplified if a constant reference value of velocity V_R is assumed in the expression for k. In this latter case, the only variable is ω and therefore $[T]$ can be written in the form

$$[T] = \begin{bmatrix} 0 & 0 \\ 0 & -1.86 \end{bmatrix} + i \frac{\omega}{\omega_R} \begin{bmatrix} a_L & \\ & a_T \end{bmatrix} \begin{bmatrix} -100 & 100 \\ 100 & 80 \end{bmatrix} \tag{32}$$

where $\omega_R = \dfrac{V_R}{b}$ is a reference frequency. Since a_L and a_T are free parameters, it is convenient to reduce the scaling of the G_{ij} element by a factor of 25 to make the maximum G_{ij} values the same as for the case of the localized damping type transfer function. Hence, equation (32) (scaled) yields the following standardized form of control law for the damping type transfer function:

$$\begin{Bmatrix} \beta \\ \delta \end{Bmatrix} = \left(\begin{bmatrix} 0 & 0 \\ 0 & -1.86 \end{bmatrix} + i \frac{\omega}{\omega_R} \begin{bmatrix} a_L & \\ & a_T \end{bmatrix} \begin{bmatrix} -4 & 4 \\ 4 & 3.2 \end{bmatrix} \right) \begin{Bmatrix} h/b \\ \alpha \end{Bmatrix} \tag{33}$$

(Note that for a given case the values of a_L and a_T in equation (33) differ from those in eq. (32).) Similarly, if

$$k_n \approx \frac{\omega_n b}{V}$$

the localized damping type transfer function can be simplified to yield the following form of standardized control law (see eq. (31)):

$$\begin{Bmatrix} \beta \\ \delta \end{Bmatrix} = \left(\begin{bmatrix} 0 & 0 \\ 0 & -1.86 \end{bmatrix} + \begin{bmatrix} \dfrac{a_L(i\omega)^2}{(i\omega)^2 + 2\zeta_L\omega_{n,L}(i\omega) + \omega_{n,L}^2} & 0 \\ 0 & \dfrac{a_T(i\omega)^2}{(i\omega)^2 + 2\zeta_T\omega_{n,T}(i\omega) + \omega_{n,T}^2} \end{bmatrix} \begin{bmatrix} -4 & 4 \\ 4 & 2.8 \end{bmatrix} \right) \begin{Bmatrix} h/b \\ \alpha \end{Bmatrix} \tag{34}$$

The similarity between the gains appearing in equation (33) and those appearing in equation (34) are now immediately apparent.

If a_L and a_T are sufficiently large to make the effect of C_{22} negligible, then equation (34) shows that the ratio between h/b gains and the α gains is 1:0.7 $\left(=\frac{4}{2.8}\right)$. Since these gains are associated with a point at 0.6b from the leading edge (30-percent chord), identical activation will be obtained by a linear sensor at 1.3b (=0.6 + 0.7) driving the trailing-edge control system. This point is at the 65-percent chord measured from the leading edge (the damping type transfer function yields a point located at 70-percent chord). For either transfer function the leading-edge control can be driven by a single sensor located at -0.4b (=0.6 - 1), or 20-percent chord ahead of the leading edge. This location is clearly not practical and, therefore, two accelerometers should be employed to drive the leading-edge control.

These generalized control laws essentially determine the relation between the gains associated with the h/b and α for each control surface irrespective of whether one or more control surfaces are actuated on the same strip. This statement implies that the relationship between the gains will be applicable to three-dimensional flows, if the ratios between the lift and the moment produced by the rotation of the respective control surface are the same as in the two-dimensional flow case.

CONCLUDING REMARKS

Control laws using realizable transfer functions are derived which permit the relaxation of the stability requirements of the aerodynamic energy approach. The resulting aerodynamic eigenvalues indicate that both the

trailing-edge and the leading-edge—trailing-edge control systems can be made more effective. As a result, flutter suppression and gust-alleviation problems can successfully be tackled by the aerodynamic energy approach with a trailing-edge control system only and without encountering sensitivity to changing flight conditions. In the original aerodynamic energy approach, such an ability could be handled by a leading-edge—trailing-edge system only.

Free parameters have been identified which control the amount of the aerodynamic damping introduced by the activated system. Furthermore, one of the control laws also permits the selection of a reduced frequency range within which damping is to be increased and provides stiffness terms for controlling the response of the system. The values of these free parameters can be tailored to specific applications. The results have been reduced to a simple form and are applicable to a very wide class of aircraft operating within the subsonic Mach number range.

Langley Research Center
National Aeronautics and Space Administration
Hampton, VA 23665
July 7, 1977

APPENDIX A

THE ENERGY ANALYSIS

Let the n equations

$$\{F\} = -\omega^2\left[B + \pi\rho b^4 s(A_R + iA_I)\right]\{\bar{q}\} + [E]\{\bar{q}\} \tag{A1}$$

represent the equations of motion of n structural modes with r activated controls, where at flutter

$$\{F\} = 0$$

and

ω frequency of oscillation

$[B]$ mass matrix

$[A_R], [A_I]$ real and imaginary parts of aerodynamic matrix, respectively

$[E]$ stiffness matrix

ρ fluid density

s reference length

b reference semichord length

All matrices in equation (A1) are of the order $n \times (n + r)$ (n structural modes and r active controls). The response vector $\{\bar{q}\}$ in terms of n structural responses and r control deflections is

$$\{\bar{q}\} = \begin{Bmatrix} q \\ q_c \end{Bmatrix} \tag{A2}$$

Equation (A1) can therefore be written as

$$\{F\} = \left(-\omega^2\left[\left[B_s \vdots B_c\right] + \pi\rho b^4 s\left(\left[A_{R,s} \vdots A_{R,c}\right] + i\left[A_{I,s} \vdots A_{I,c}\right]\right)\right] + \left[E_s \vdots E_c\right]\right)\begin{Bmatrix} q \\ q_c \end{Bmatrix} \tag{A3}$$

APPENDIX A

Assume a control law of the form

$$\{q_c\} = [T]\{q\} \tag{A4}$$

where $[T]$ is a r × n matrix representing the transfer functions of the control law. By substituting equation (A4) into equation (A3), the following equation is obtained:

$$\{F\} = \left(-\omega^2\left[[B_s] + [B_c][T] + \pi\rho b^4 s\left([A_{R,s}] + [A_{R,c}][T] + i[A_{I,s}] + i[A_{I,c}][T]\right)\right] + [E_s] + [E_c][T]\right)\{q\} \tag{A5}$$

where the products $[B_c][T]$, $[A_{R,c}][T]$, $[A_{I,c}][T]$, and $[E_c][T]$ are now n × n matrices. The vector $\{q\}$ can be written as

$$\{q\} = \{q_o\}e^{i\omega t} = \{q_R + iq_I\}e^{i\omega t} \tag{A6}$$

The real part of equation (A5) is essentially the same as the imaginary part, except for the initial conditions at $t = 0$. In harmonic motion, where no transients are treated, only the real part of equation (A1) need be considered. Hence, the forces which the system exerts on its surroundings are given by

$$\begin{aligned}\{F\} = {} & \frac{1}{2}\left(-\omega^2\left[[B_s] + [B_c][T] + \pi\rho b^4 s\left([A_{R,s}] + [A_{R,c}][T] + i[A_{I,s}] + i[A_{I,c}][T]\right)\right] + [E_s] + [E_c][T]\right)\{q_o\}e^{i\omega t} \\ & + \frac{1}{2}\left(-\omega^2\left[[B_s] + [B_c][T^*] + \pi\rho b^4 s\left([A_{R,s}] + [A_{R,c}][T^*] - i[A_{I,s}] - i[A_{I,c}][T^*]\right)\right] + [E_s] + [E_c][T^*]\right)\{q_o^*\}e^{-i\omega t}\end{aligned} \tag{A7}$$

where the asterisk denotes the conjugate vector. The vector $\{F\}$ is clearly a real vector.

APPENDIX A

The velocity vector $\{\dot{q}\}$ can be obtained by differentiating equation (A6) to obtain

$$\{\dot{q}\} = i\omega\{q_o\}e^{i\omega t} \tag{A8}$$

The real part of the velocity vector $R(\dot{q})$ is given by

$$R\{\dot{q}\} = \frac{1}{2} i\omega\{q_o\}e^{i\omega t} - \frac{1}{2} i\omega\{q_o^*\}e^{-i\omega t} \tag{A9}$$

Hence, the rate at which the system does work on its surroundings is given by $R\lfloor\dot{q}\rfloor\{F\}$. Equations (A7) and (A9) yield

$$\begin{aligned}
R\lfloor\dot{q}\rfloor\{F\} = {} & \frac{i\omega}{4}\lfloor q_o\rfloor\Big(-\omega^2\Big[\big[B_s\big] + \big[B_c\big]\big[T\big] + \pi\rho b^4 s\Big(\big[A_{R,s}\big] + \big[A_{R,c}\big]\big[T\big] \\
& + i\big[A_{I,s}\big] + i\big[A_{I,c}\big]\big[T\big]\Big)\Big] + \big[E_s\big] + \big[E_c\big]\big[T\big]\Big)\{q_o\}e^{2i\omega t} \\
& - \frac{i\omega}{4}\lfloor q_o^*\rfloor\Big(-\omega^2\Big[\big[B_s\big] + \big[B_c\big]\big[T\big] + \pi\rho b^4 s\Big(\big[A_{R,s}\big] + \big[A_{R,c}\big]\big[T\big] \\
& + i\big[A_{I,s}\big] + i\big[A_{I,c}\big]\big[T\big]\Big)\Big] + \big[E_s\big] + \big[E_c\big]\big[T\big]\Big)\{q_o\} \\
& + \frac{i\omega}{4}\lfloor q_o\rfloor\Big(-\omega^2\Big[\big[B_s\big] + \big[B_c\big]\big[T^*\big] + \pi\rho b^4 s\Big(\big[A_{R,s}\big] + \big[A_{R,c}\big]\big[T^*\big] \\
& - i\big[A_{I,s}\big] - i\big[A_{I,c}\big]\big[T^*\big]\Big)\Big] + \big[E_s\big] + \big[E_c\big]\big[T^*\big]\Big)\{q_o^*\} \\
& - \frac{i\omega}{4}\lfloor q_o^*\rfloor\Big(-\omega^2\Big[\big[B_s\big] + \big[B_c\big]\big[T^*\big] + \pi\rho b^4 s\Big(\big[A_{R,s}\big] + \big[A_{R,c}\big]\big[T^*\big] \\
& - i\big[A_{I,s}\big] - i\big[A_{I,c}\big]\big[T^*\big]\Big)\Big] + \big[E_s\big] + \big[E_c\big]\big[T^*\big]\Big)\{q_o^*\}e^{-2i\omega t}
\end{aligned} \tag{A10}$$

Hence, the work P done per cycle by the system on its surroundings can be found by integrating equation (A10) between $t = 0$ and $t = 2\pi/\omega$. Thus,

$$P = \frac{i\pi}{2}\lfloor q_o \rfloor \Big(-\omega^2 \Big[[B_s] + [B_c][T^*] + \pi\rho b^4 s \Big([A_{R,s}] + [A_{R,c}][T^*] - i[A_{I,s}] - i[A_{I,c}][T^*] \Big) \Big] + [E_s] + [E_c][T^*] \Big) \{q_o^*\}$$

$$- \frac{i\pi}{2}\lfloor q_o^* \rfloor \Big(-\omega^2 \Big[[B_s] + [B_c][T] + \pi\rho b^4 s \Big([A_{R,s}] + [A_{R,c}][T] + i[A_{I,s}] + i[A_{I,c}][T] \Big) \Big] + [E_s] + [E_c][T] \Big) \{q_o\}$$

This equation is a scalar equation; therefore, the first expression on the right-hand side of this equation can be transposed ($[B_s]$ and $[E_s]$ being assumed to be symmetric)

$$P = \frac{\pi^2\rho b^4\omega^2 s}{2}\lfloor q_o^* \rfloor \Big[-\Big([A_{I,s}] + [A_{I,s}]^T + [A_{I,c}][T] + [T^*]^T[A_{I,c}]^T \Big) + i\Big([A_{R,s}] - [A_{R,s}]^T + [A_{R,c}][T] - [T^*]^T[A_{I,c}]^T \Big) \Big] \{q_o\}$$

$$+ \frac{\pi\omega^2}{2}\lfloor q_o^* \rfloor \Big[i\Big([B_c][T] - [T^*]^T[B_c]^T \Big) \Big] \{q_o\}$$

$$+ \frac{\pi}{2}\lfloor q_o^* \rfloor \Big[i\Big([E_c][T] - [T^*]^T[E_c]^T \Big) \Big] \{q_o\} \qquad \text{(A11)}$$

The matrix $[E_c]$ is assumed to be zero since, in general, no elastic couplings exist between the structural modes and the control deflections. Hence, equation (A11) reduces to

APPENDIX A

$$P = \frac{\pi^2 \rho b^4 \omega^2 s}{2} \{q_o^*\} \left[-\left([A_{I,s}] + [A_{I,s}]^T + [A_{I,c}][T] + [T^*]^T [A_{I,c}]^T \right) \right.$$

$$+ i \left(\frac{[B_c][T] - [T^*]^T [B_c]^T}{\pi \rho b^4 s} + [A_{R,s}] - [A_{R,s}]^T \right.$$

$$\left. \left. + [A_{R,c}][T] - [T^*]^T [A_{R,c}]^T \right) \right] \{q_o\} \tag{A12}$$

Note that the matrices within the square brackets form a Hermitian matrix.

Now determine the eigenvalues and eigenvectors of the following Hermitian matrix $[U]$ extracted from equation (A12):

$$\lambda\{\eta\} = [U]\{\eta\} \tag{A13}$$

where

$$[U] = \left[-\left([A_{I,s}] + [A_{I,s}]^T + [A_{I,c}][T] + [T^*]^T [A_{I,c}]^T \right) \right.$$

$$+ i \left(\frac{[B_c][T] - [T^*]^T [B_c]^T}{\pi \rho b^4 s} + [A_{R,s}] - [A_{R,s}]^T \right.$$

$$\left. \left. + [A_{R,c}][T] - [T^*]^T [A_{R,c}]^T \right) \right] \tag{A14}$$

and represent the vector $\{q_o\}$ in terms of the eigenvectors of equation (A13), that is,

$$\{q_o\} = [Q_R + iQ_i]\{\xi_R + i\xi_I\} \tag{A15}$$

The columns of the square matrices $[Q_R]$ and $[Q_I]$ are the real and imaginary parts of the eigenvectors of equation (A13). The vector $\{\xi_R + i\xi_I\}$ contains the generalized modal coordinates of the transformation defined by equation (A15).

All the eigenvalue and eigenvector solutions of equation (A13) can be expressed in the form $[Q_R + iQ_I][\lambda] = [U][Q_R + iQ_I]$. Postmultiplying this

equation by $\{\xi_R + i\xi_I\}$ and premultiplying it by $\lfloor q_o^* \rfloor$ or $\lfloor \xi_R - i\xi_I \rfloor [Q_R^T - iQ_I^T]$ yields

$$\lfloor \xi_R - i\xi_I \rfloor [Q_R^T - iQ_I^T] [Q_R + iQ_I] [\lambda] \{\xi_R + i\xi_I\}$$

$$= \lfloor \xi_R - i\xi_I \rfloor [Q_R^T - iQ_I^T] \left[-\left([A_{I,s}] + [A_{I,s}]^T + [A_{I,c}][T] \right.\right.$$

$$\left. + [T^*]^T [A_{I,c}]^T \right) + i \left(\frac{[B_c][T] - [T^*]^T [B_c]^T}{\pi \rho b^4 s} + [A_{R,s}] - [A_{R,s}]^T \right.$$

$$\left.\left. + [A_{R,c}][T] - [T^*]^T [A_{R,c}]^T \right) \right] [Q_R + iQ_I] \{\xi_R + i\xi_I\} \tag{A16}$$

where $[\lambda]$ is the eigenvalue matrix, that is,

$$[\lambda] = \begin{bmatrix} \lambda_1 & & & \\ & \lambda_2 & & \\ & & \ddots & \\ & & & \lambda_n \end{bmatrix} \tag{A17}$$

The right-hand side of equation (A16) is identical to the right-hand side of equation (A12) except for the $\pi^2 \rho b^4 \omega^2 s/2$ factor. Hence, the left-hand sides of these two equations can be equated to obtain

$$P = \frac{\pi^2 \rho b^4 \omega^2 s}{2} \lfloor \xi_R - i\xi_I \rfloor [Q_R^T - iQ_I^T] [Q_R + iQ_I] \{\xi_R + i\xi_I\}$$

The matrix $[Q_R^T - iQ_I^T]$ represents the modal matrix of the complex left-hand normalized eigenvectors and therefore

$$[Q_R^T - iQ_I^T] [Q_R + iQ_I] = [I] \tag{A18}$$

where $[I]$ is the unit matrix. Hence, P reduces to the form

$$P = \frac{\pi^2 \rho b^4 \omega^2 s}{2} \lfloor \xi_R - i\xi_I \rfloor [\lambda] \{\xi_R + i\xi_I\} \tag{A19}$$

or

$$P = \frac{\pi^2 \rho b^4 \omega^2 s}{2} \left(\lfloor \xi_R \rfloor [\lambda] \{\xi_R\} + \lfloor \xi_I \rfloor [\lambda] \{\xi_I\} \right) \tag{A20}$$

The energy input per cycle into the surroundings has thus been reduced to a quadratic form in terms of the generalized energy modal coordinates.

Note that if all control surfaces are mass balanced, the matrix $[B_c]$ vanishes and $[U]$ reduces to

$$[U] = \left[-\left([A_{I,s}] + [A_{I,s}]^T + [A_{I,c}][T] + [T^*]^T [A_{I,c}]^T \right) + i\left([A_{R,s}] - [A_{R,s}]^T + [A_{R,c}][T] - [T^*]^T [A_{R,c}]^T \right) \right] \tag{A21}$$

when the control system is not activated $[T] = 0$ and

$$[U] = \left[-\left([A_{I,s}] + [A_{I,s}]^T \right) + i\left([A_{R,s}] - [A_{R,s}]^T \right) \right] \tag{A22}$$

APPENDIX B

CONVERSION OF STRUCTURAL DAMPING INTO EQUIVALENT AERODYNAMIC EIGENVALUES

Let the structural damping force $F_{d,i}$ acting on the ith structural mode be expressed by

$$F_{d,i} = ig_i\omega_{n,i}^2 b_R m_i q_i \tag{B1}$$

where

g_i structural damping coefficient of ith mode

$\omega_{n,i}$ natural frequency of ith mode

m_i generalized mass of ith mode

b_R reference wing semichord

q_i nondimensional generalized modal response

The work W done by the damping force per cycle of oscillation is given by

$$W = \int_0^{2\pi/\omega} F_s \frac{dq_i}{dt}\, dt \tag{B2}$$

Substitution of equation (B1) into equation (B2) yields

$$W = g_i\omega_{n,i}^2 b_R^2 m_i \int_0^{2\pi/\omega} iq \frac{dq}{dt}\, dt \tag{B3}$$

Let

$$q_i = q_{o,i} \sin \omega t \tag{B4}$$

$$iq_i = \frac{\dot{q}_i}{\omega} = q_{o,i} \cos \omega t \tag{B5}$$

Therefore,

$$W = \pi g_i \omega_{n,i}^2 b_R^2 m_i q_{o,i}^2 \tag{B6}$$

Let the work done per cycle be defined in a form equivalent to the newly defined aerodynamic eigenvalues, that is,

$$W = \frac{1}{2} \pi^2 \rho b_c^2 V^2 s_c \lambda_{d,i} q_{o,i}^2 = \pi g_i \omega_{n,i}^2 b_R^2 m_i q_{o,i}^2 \tag{B7}$$

where b_c is the semichord at the control-surface midspan region, s_c is the control-surface span, and $\lambda_{d,i}$ is the equivalent value of the structural damping in terms of the aerodynamic type eigenvalues. Equation (B7) yields

$$\lambda_{d,i} = \frac{2 g_i \omega_{n,i}^2 b_R^2 m_i}{\pi \rho b_c^2 V^2 s_c} \tag{B8}$$

Define the mass ratio $M_{R,i}$ as

$$M_{R,i} = \frac{m_i}{\pi \rho b_R^2 s} \tag{B9}$$

Substitution of equation (B9) into equation (B8) yields

$$\lambda_{d,i} = 2 g_i \left(\frac{b_R}{b_c} \right)^4 \frac{s}{s_c} k_{n,c,i}^2 M_{R,i} \tag{B10}$$

where $k_{n,c,i}$ is defined by

$$k_{n,c,i} = \frac{\omega_{n,i} b_c}{V} \tag{B11}$$

For a two-dimensional strip $s = s_c$ and $b_R = b_c$. Equation (B10) reduces in this case to

$$\lambda_{d,i} = 2g_i k_{n,c,i}^2 M_{R,i} \tag{B12}$$

REFERENCES

1. Nissim, E.: Flutter Suppression Using Active Controls Based on the Concept of Aerodynamic Energy. NASA TN D-6199, 1971.

2. Sandford, Maynard C.; Abel, Irving; and Gray, David L: Development and Demonstration of a Flutter-Suppression System Using Active Controls. NASA TR R-450, 1975.

3. Nissim, E.; Caspi, A.; and Lottati, I.: Application of the Aerodynamic Energy Concept to Flutter Suppression and Gust Alleviation by Use of Active Controls. NASA TN D-8212, 1976.

4. Stewart, G. W., III: A Modification of Davidon's Minimization Method To Accept Difference Approximations of Derivatives. J. Assoc. Comput. Mach., vol. 14, no. 1, Jan. 1967, pp. 72-82.

5. Fletcher, R.; and Powell, M. J. D.: A Rapidly Convergent Descent Method for Minimization. Comput. J., vol. 6, no. 2, July 1963, pp. 163-168.

6. Nissim, E.: Flutter Suppression and Gust Alleviation Using Active Controls. TAE Rep. No. 198, Technion-Israel Inst. Technol., 1974. (Available as NASA CR-138658.)

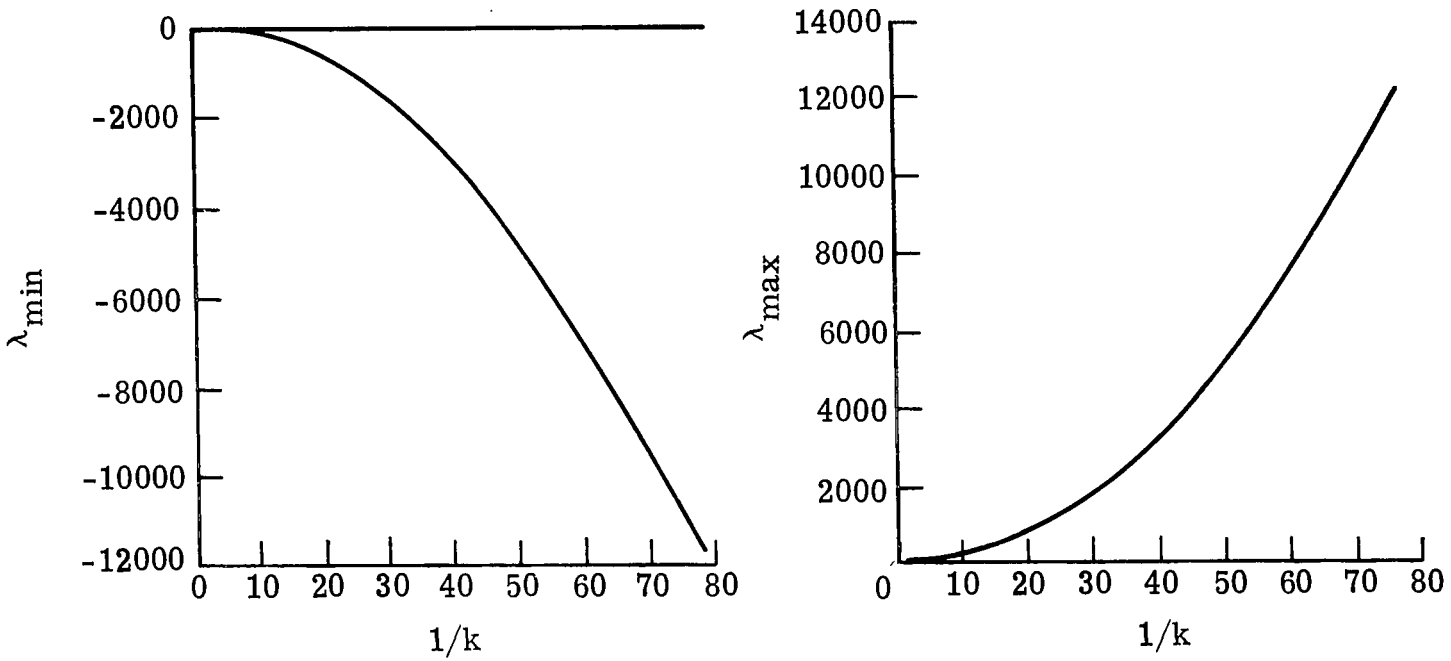

(a) λ_{min}.

(b) λ_{max}.

Figure 1.- Variation of λ (as defined by eq. (8)) with $1/k$ of a wing strip with no control surfaces. M = 0.

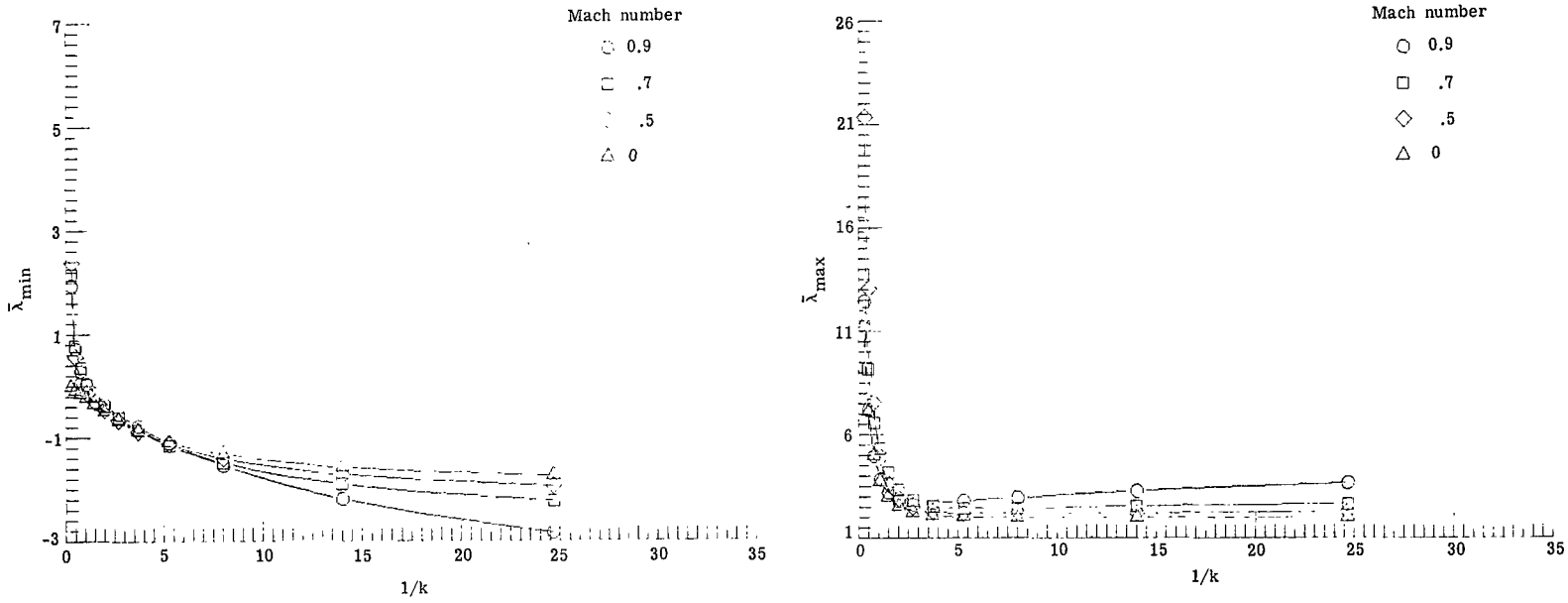

Figure 2.- Variation of $\bar{\lambda}$ with 1/k at various Mach numbers for a wing strip with no control surfaces.

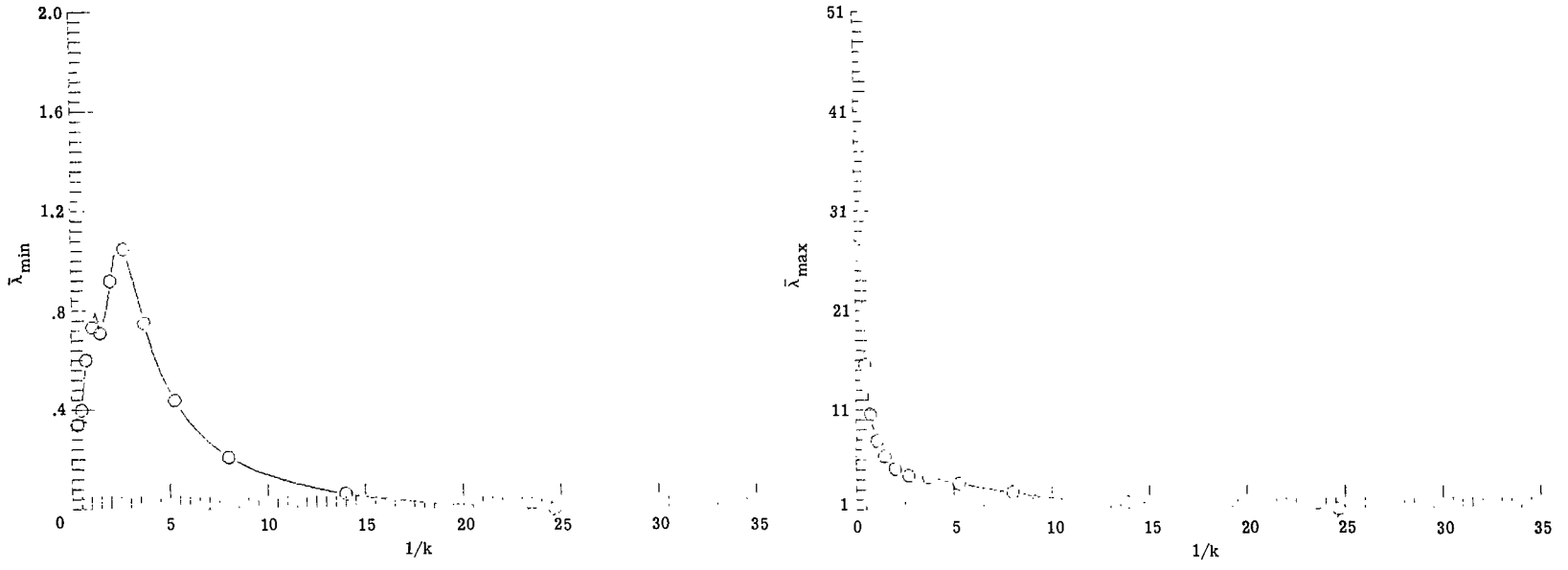

(a) $\bar{\lambda}_{min}$.

(b) $\bar{\lambda}_{max}$.

Figure 3.- Optimum variation of $\bar{\lambda}$ with $1/k$ for a trailing-edge control system at $M = 0.9$ (with gains optimized on the basis of λ_{min} only) using damping type transfer function.

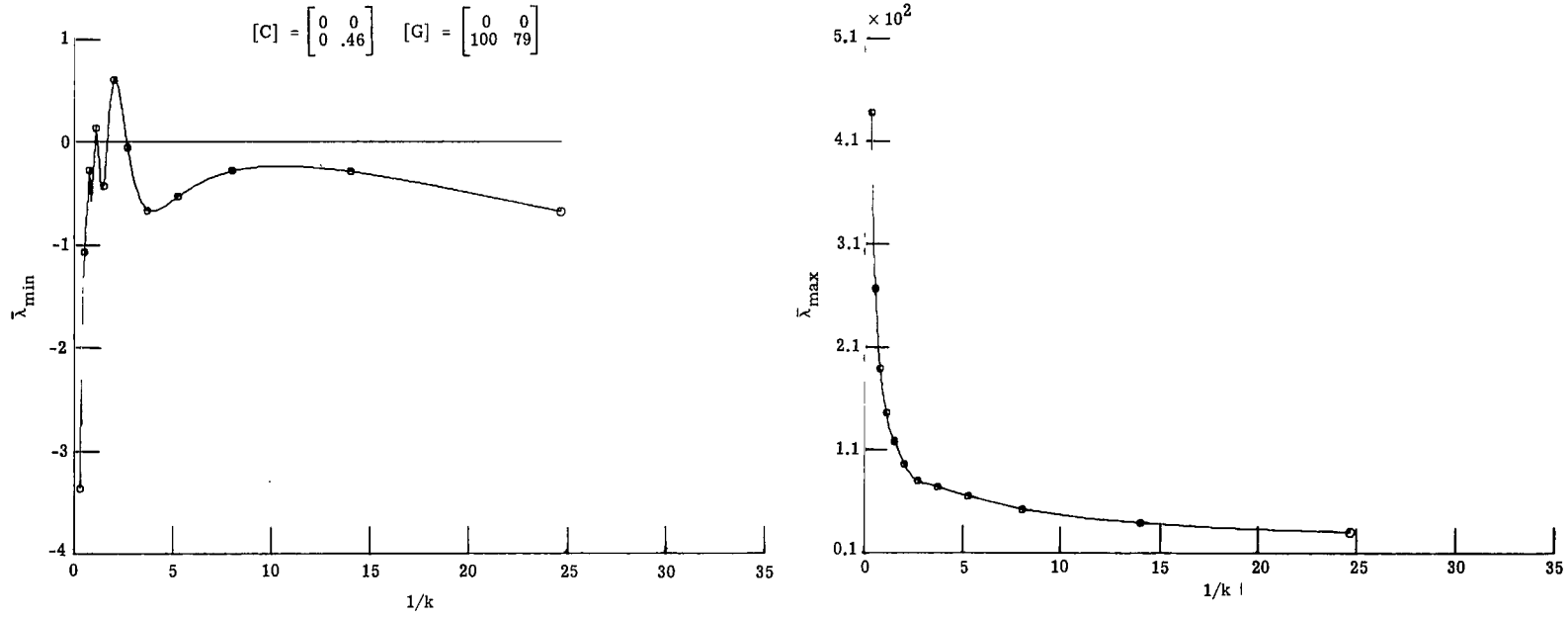

(a) $\bar{\lambda}_{min}$.

(b) $\bar{\lambda}_{max}$.

Figure 4.- Optimum variation of λ with $1/k$ for a trailing-edge control system at $M = 0.9$ (with $G_{21} = 100$) using damping type transfer function.

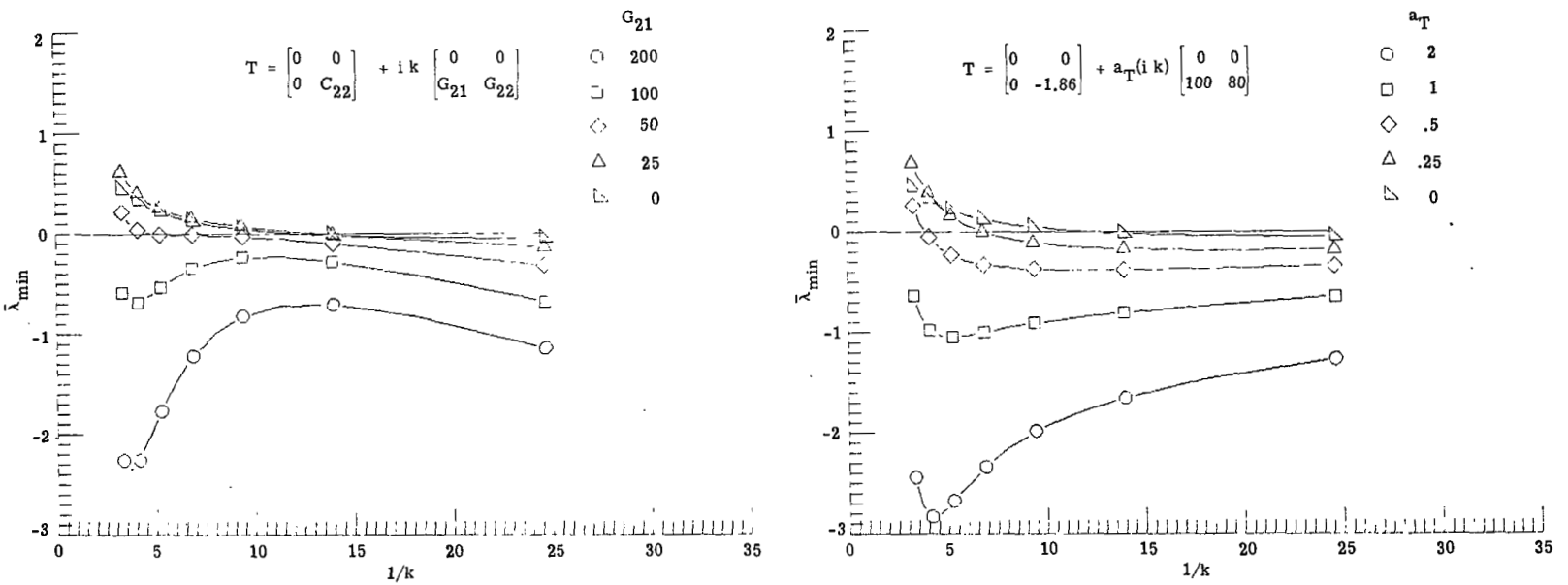

(a) Optimized gains.

(b) Fixed gains.

Figure 5.- Variation of $\bar{\lambda}_{min}$ with $1/k$ using optimized gains for different $|G_{ij}|$ ranges compared with a similar variation using fixed gains scaled by a_T. Trailing-edge control system at $M = 0.9$ and using damping type transfer function.

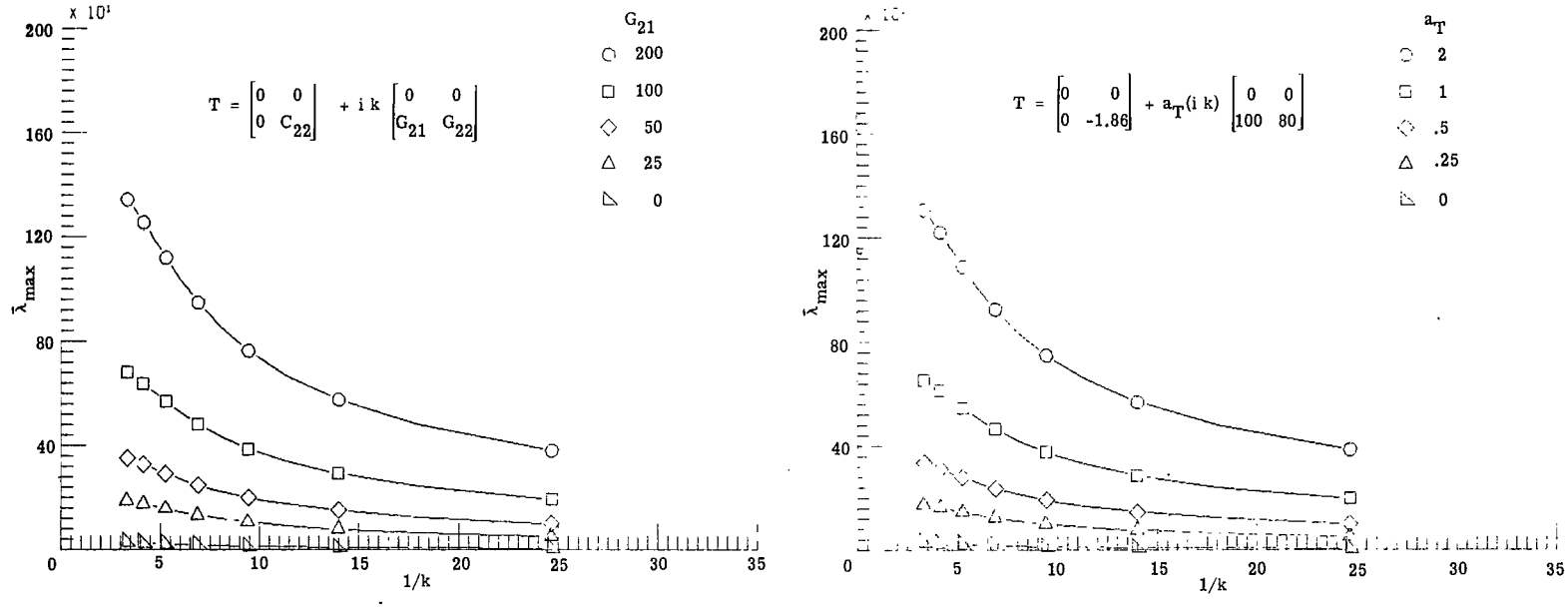

(a) Optimized gains.

(b) Scaled gains.

Figure 6.- Variation of $\bar{\lambda}_{max}$ with 1/k using optimized gains for different $|G_{ij}|$ ranges compared with a similar variation using scaled gains, trailing-edge control system at M = 0.9, and damping type transfer function.

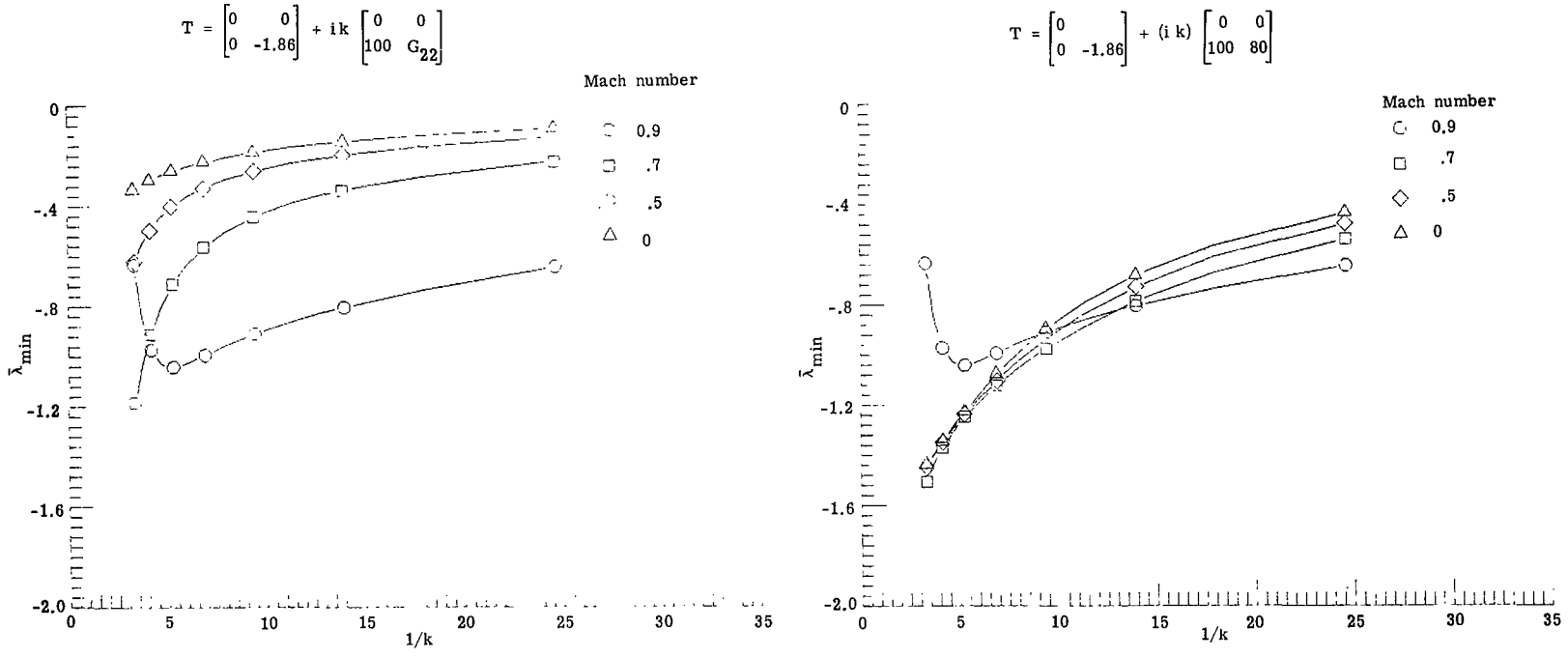

(a) Optimized gains.

(b) Fixed gains.

Figure 7.- Variation of $\bar{\lambda}_{min}$ with 1/k using optimized gains at different Mach numbers compared with a similar variation using fixed gains, trailing-edge control system, and damping type transfer function.

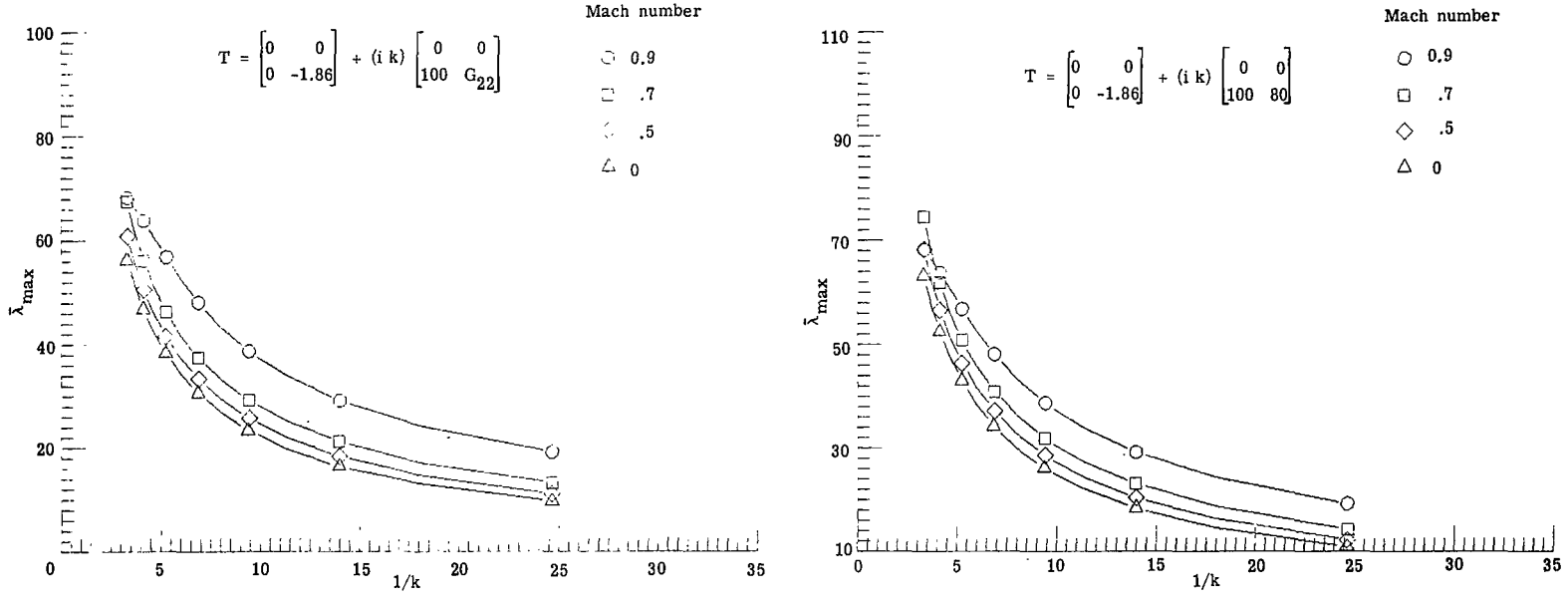

(a) Optimized gains.

(b) Fixed gains.

Figure 8.- Variation of $\bar{\lambda}_{max}$ with 1/k using optimized gains at different Mach numbers compared with a similar variation using fixed gains, trailing-edge control system, and damping type transfer function.

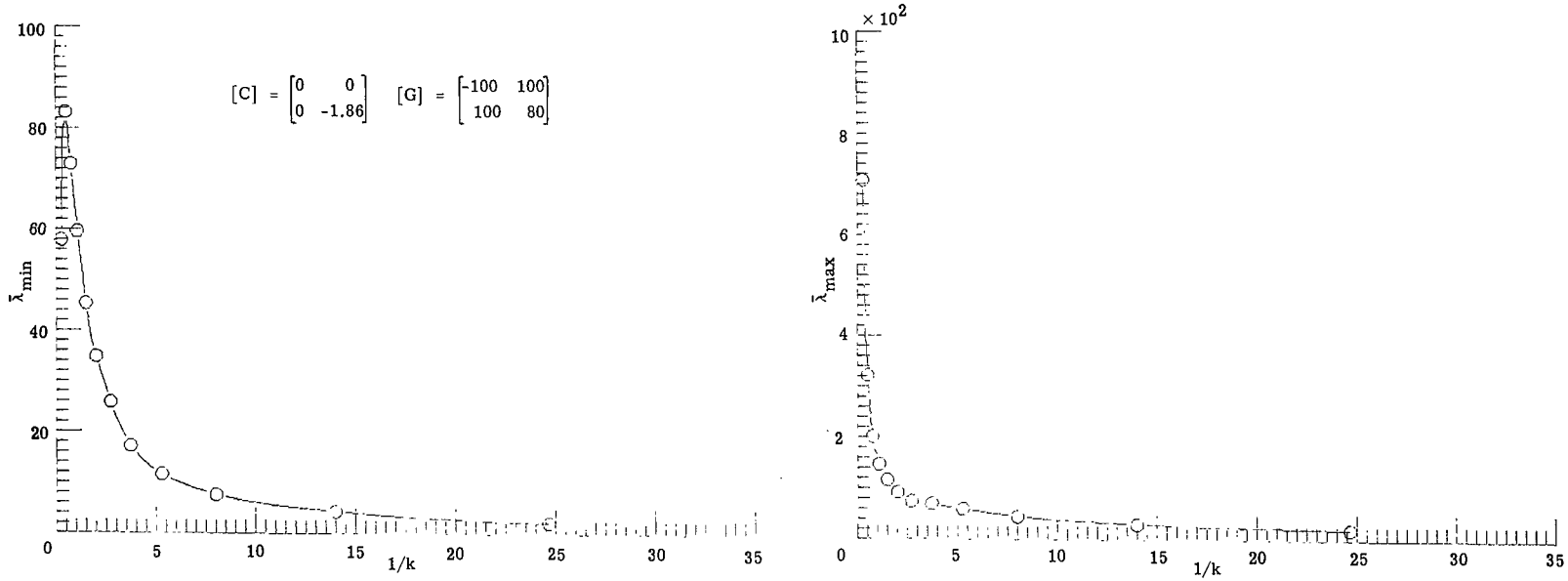

(a) $\bar{\lambda}_{min}$.

(b) $\bar{\lambda}_{max}$.

Figure 9.- Optimum variation of $\bar{\lambda}$ with 1/k for a leading-edge—trailing-edge control system at M = 0.9 (with G_{21} = 100) using damping type transfer function.

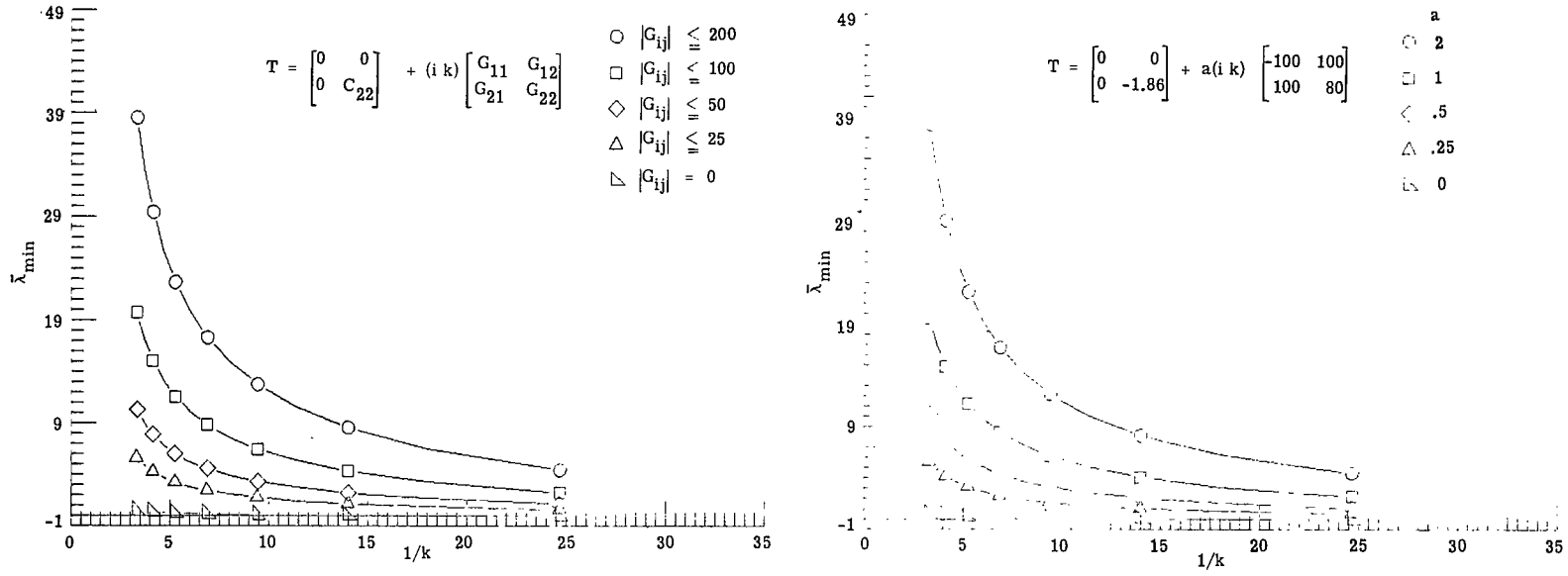

(a) Optimized gains.

(b) Scaled gains.

Figure 10.- Variation of $\bar{\lambda}_{min}$ with 1/k using optimized gains for different $|G_{ij}|$ ranges compared with a similar variation using scaled $|G_{ij}|$ gains, leading-edge—trailing-edge control system at M = 0.9, and damping type transfer function.

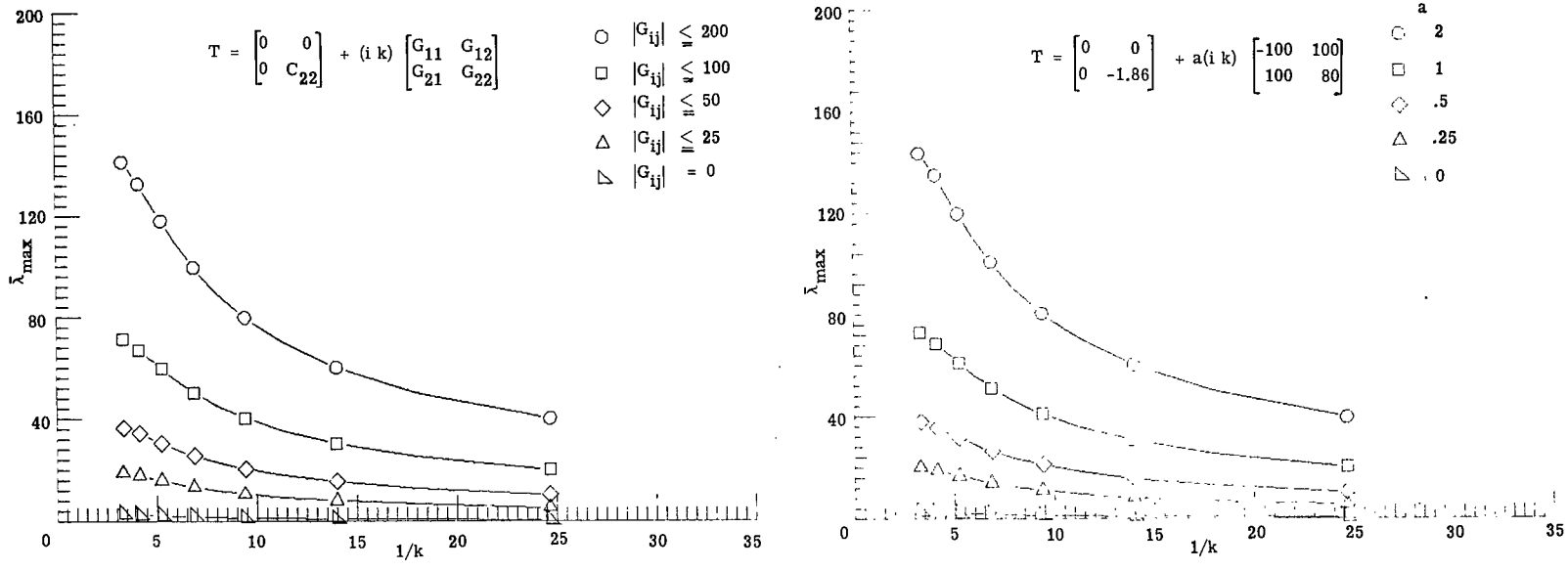

(a) Optimized gains.

(b) Scaled gains.

Figure 11.- Variation of $\bar{\lambda}_{max}$ with 1/k using optimized gains for different $|G_{ij}|$ ranges compared with a similar variation using scaled $|G_{ij}|$ gains, leading-edge—trailing-edge control system at M = 0.9, and damping type transfer function.

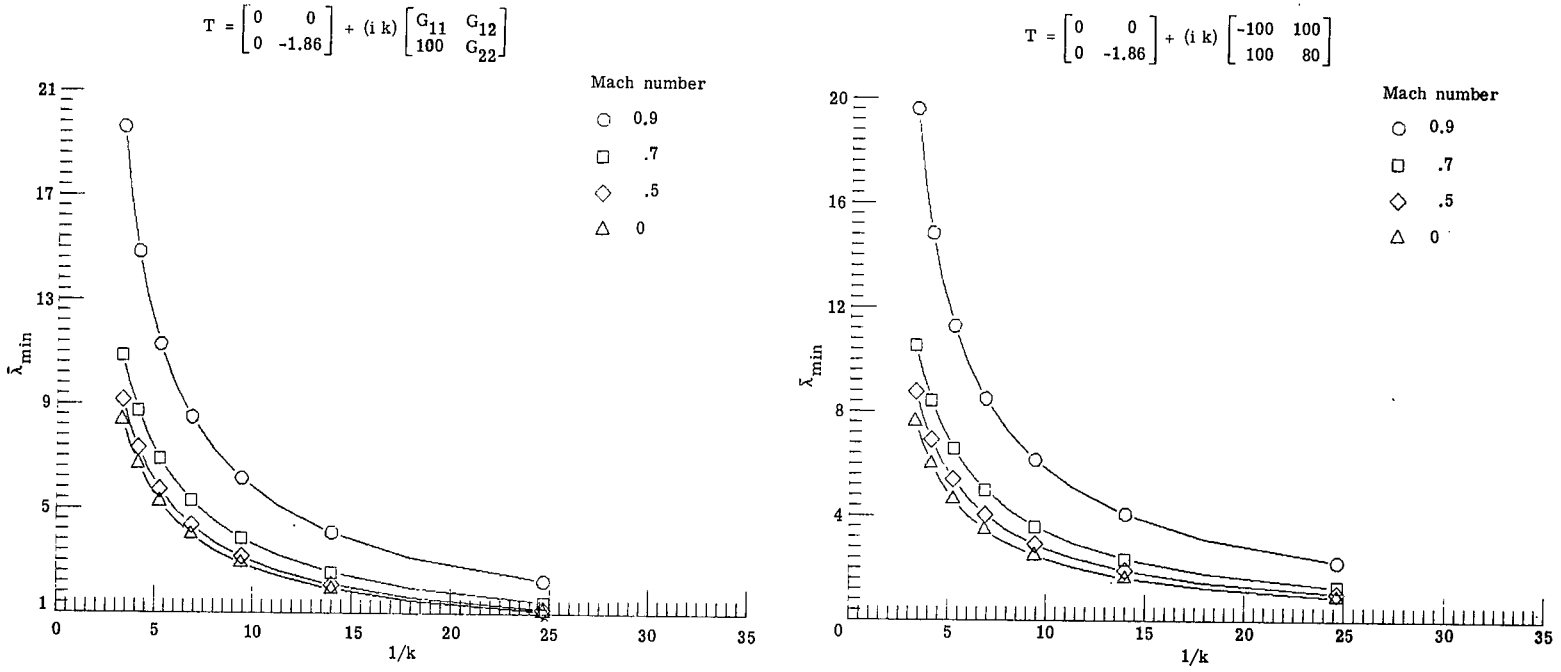

(a) Optimized gains.

(b) Fixed gains.

Figure 12.- Variation of $\bar{\lambda}_{min}$ with 1/k using optimized gains at different Mach numbers compared with a similar variation using fixed gains, leading-edge—trailing-edge control system, and damping type transfer function.

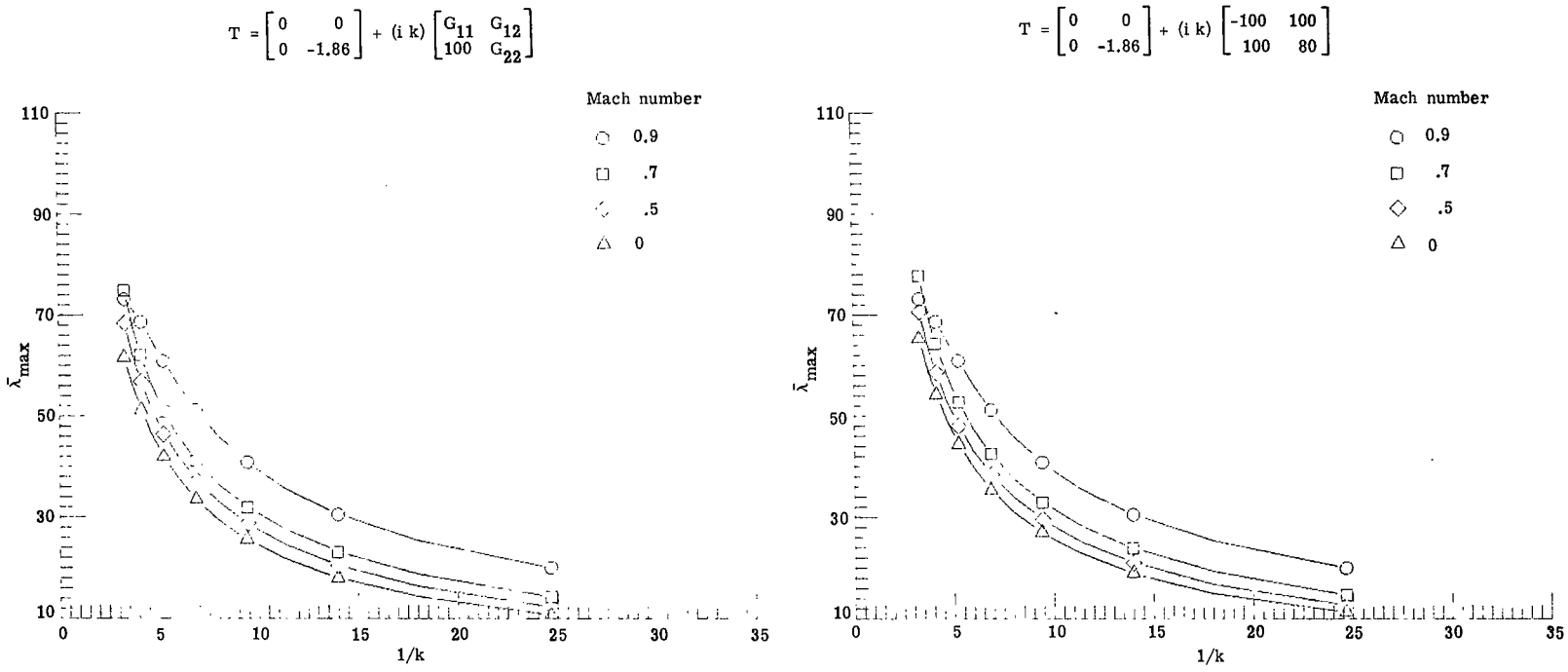

(a) Optimized gains.

(b) Fixed gains.

Figure 13.- Variation of $\bar{\lambda}_{max}$ with 1/k using optimized gains at different Mach numbers compared with a similar variation using fixed gains, leading-edge—trailing-edge control system, and damping type transfer function.

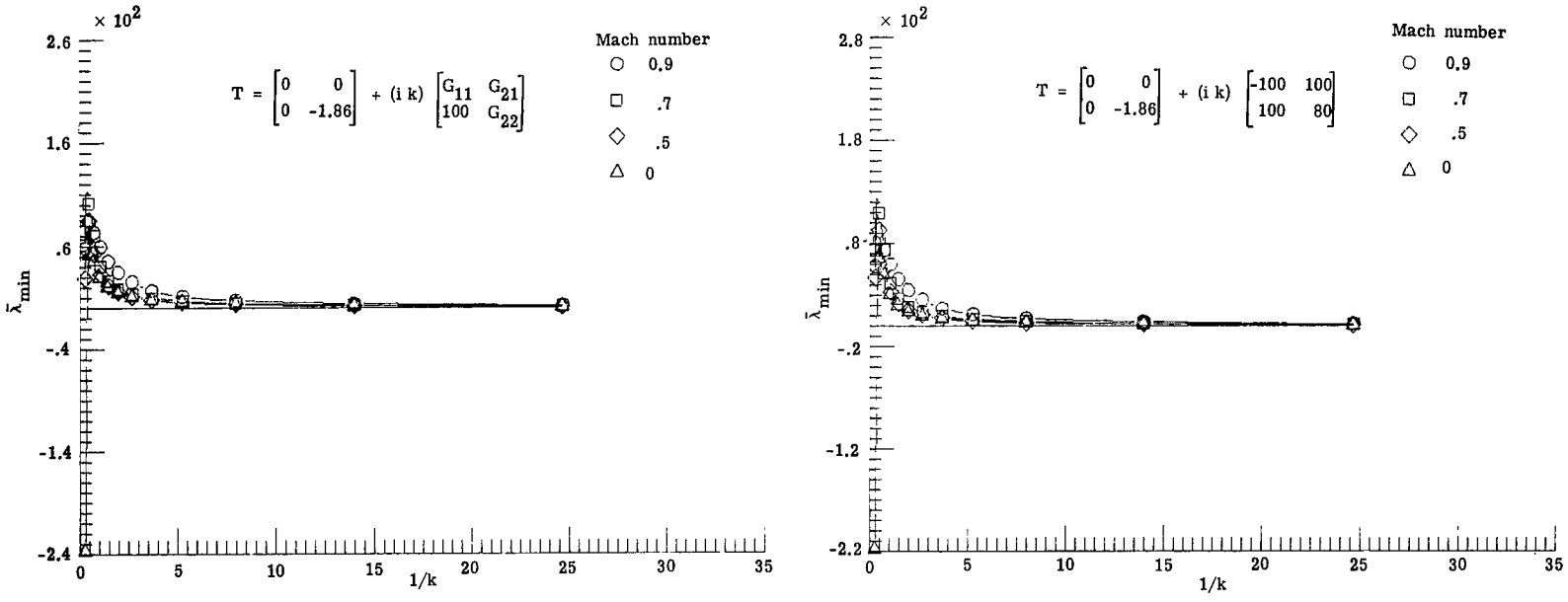

(a) Optimized gains.

(b) Fixed gains.

Figure 14.- Variation of $\bar{\lambda}_{min}$ with 1/k using optimized gains at different Mach numbers compared with a similar variation using fixed gains, leading-edge—trailing-edge control system, and damping type transfer function.

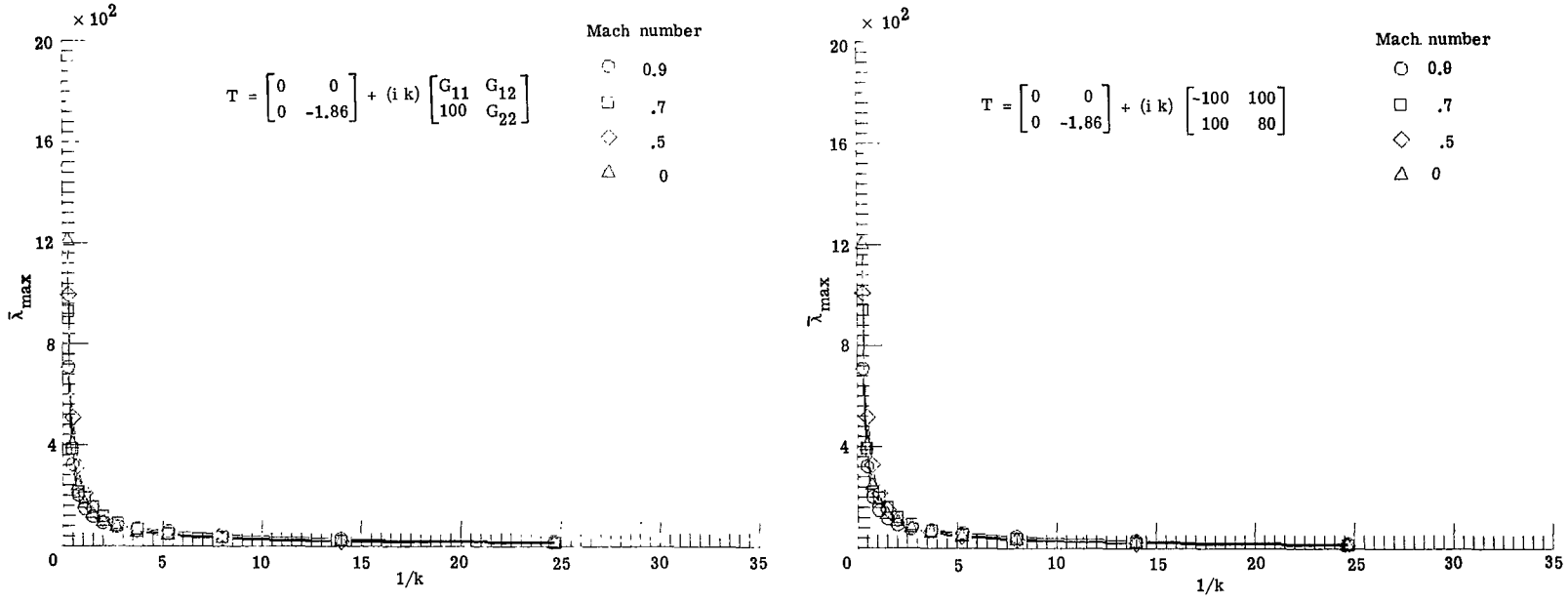

(a) Optimized gains.

(b) Fixed gains.

Figure 15.- Variation of $\bar{\lambda}_{max}$ with $1/k$ using optimized gains at different Mach numbers compared with a similar variation using fixed gains, leading-edge—trailing-edge control system, and damping type transfer function.

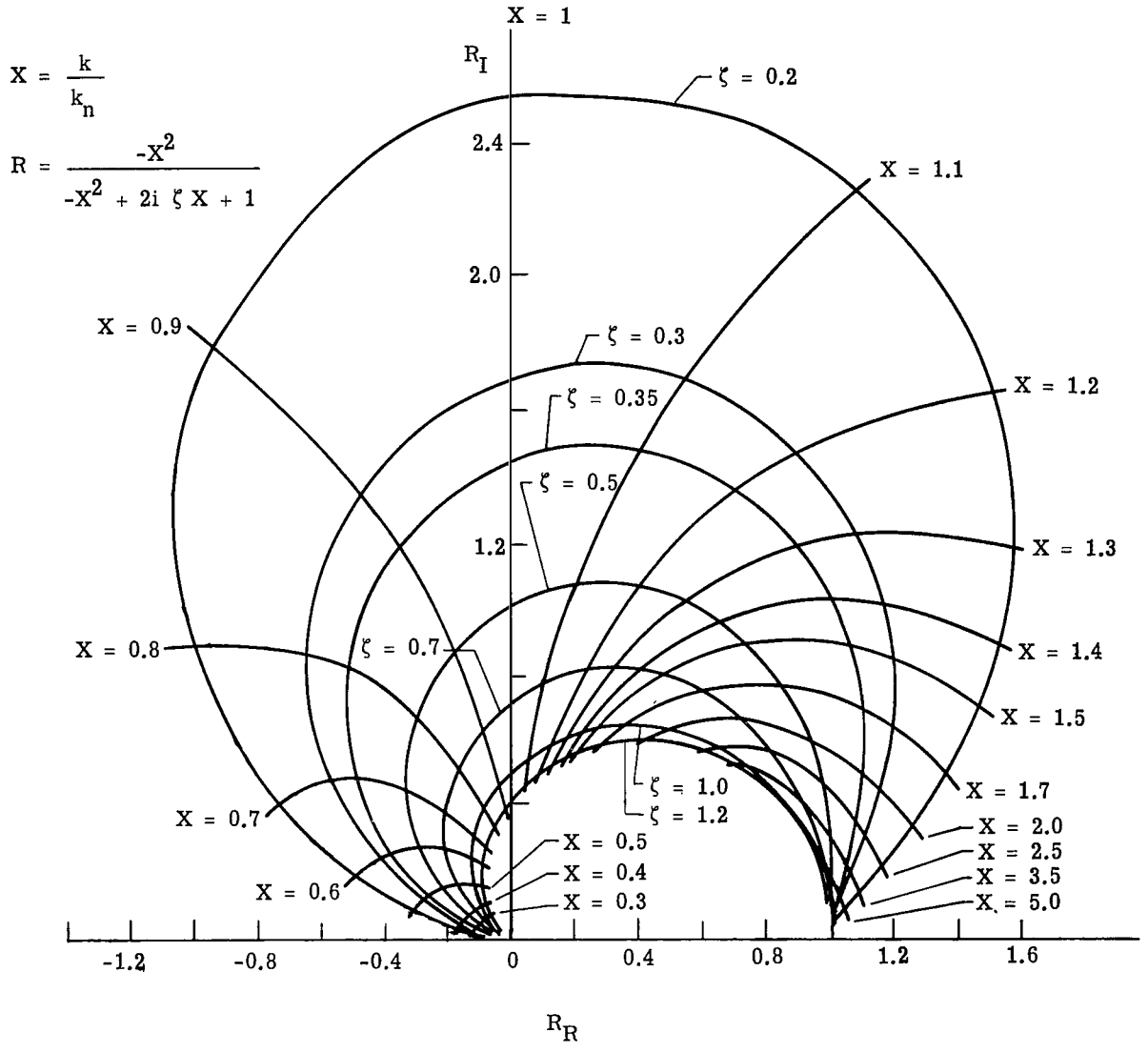

Figure 16.- Graphical representation of localized damping type transfer function.

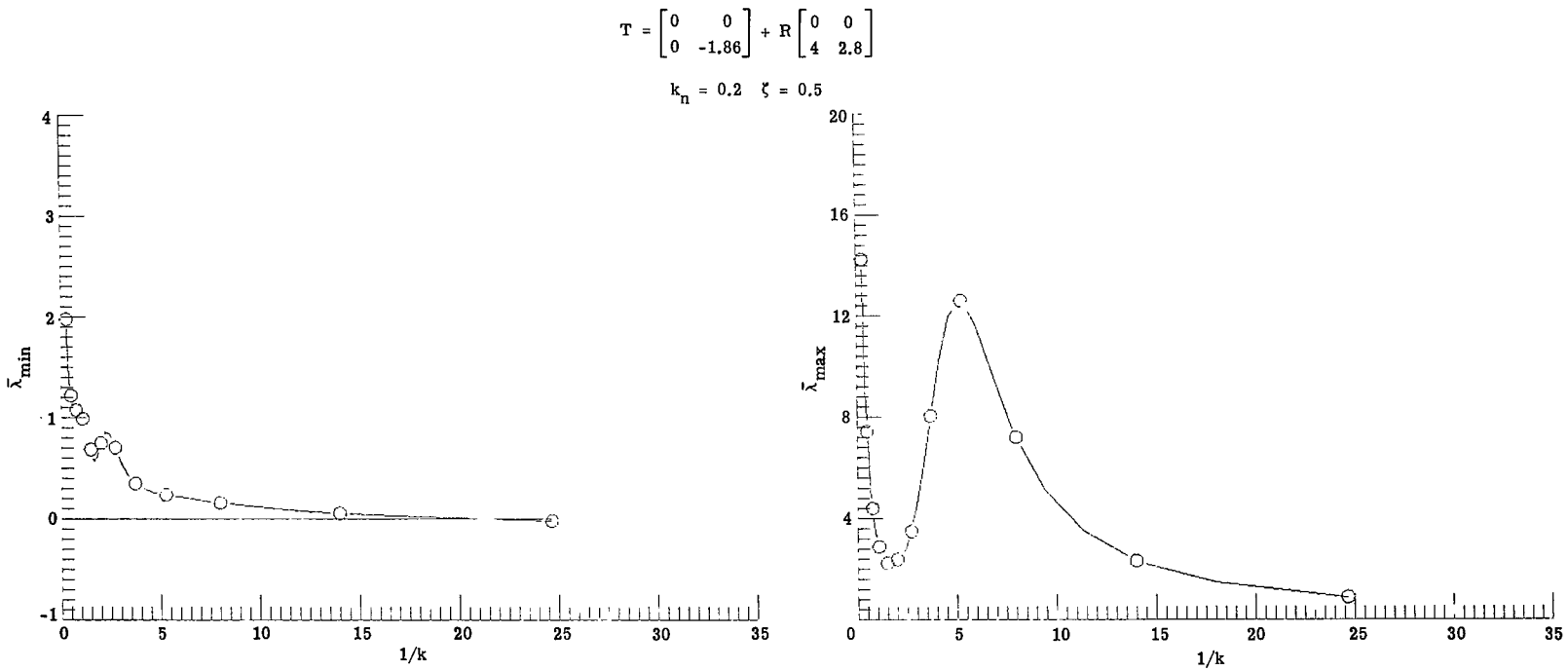

(a) $\bar{\lambda}_{min}$.

(b) $\bar{\lambda}_{max}$.

Figure 17.- Optimum variation of $\bar{\lambda}$ with 1/k for a trailing-edge control system at M = 0.9 (with G_{21} = 4) and using localized damping type transfer function.

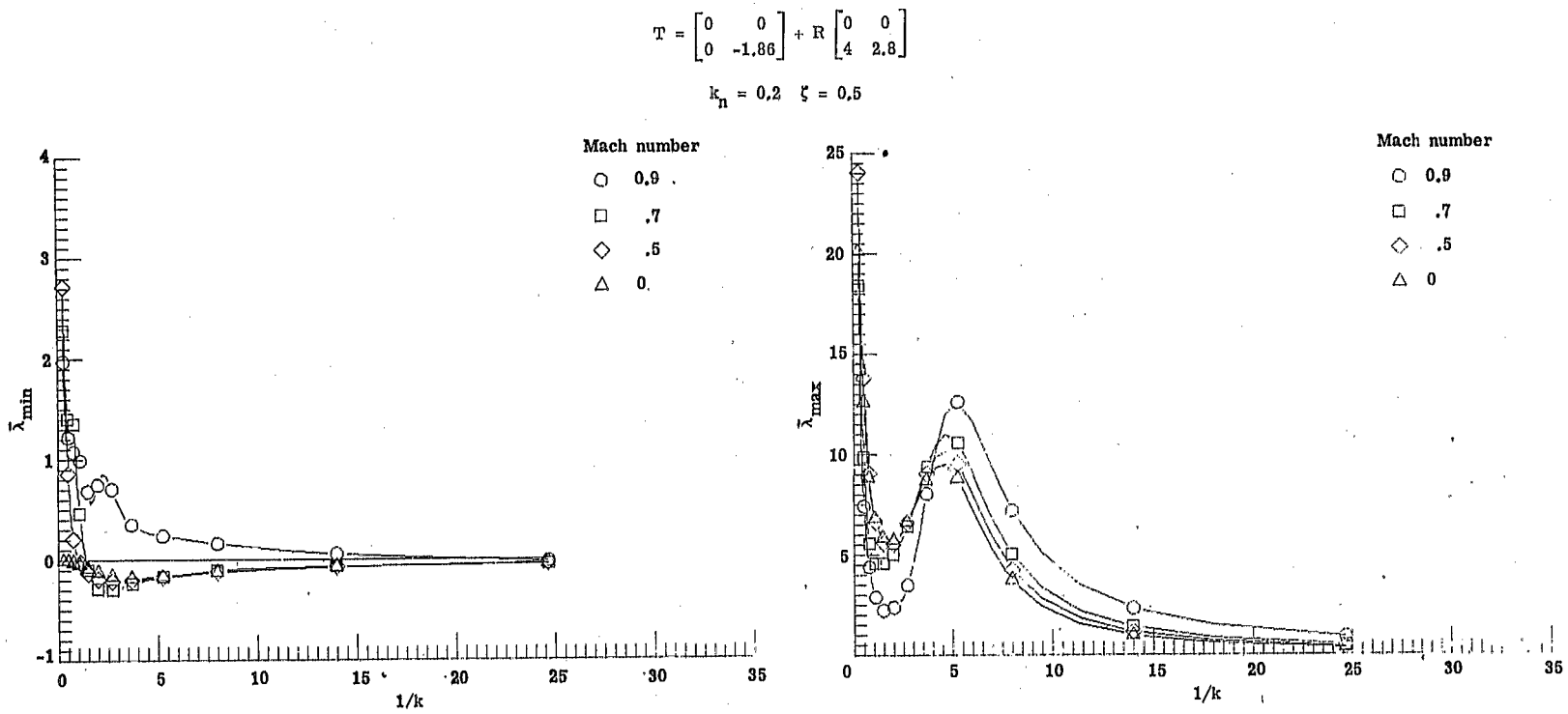

Figure 18.- Variation of $\bar{\lambda}$ with 1/k at different Mach numbers. Trailing-edge control system using localized damping type transfer function.

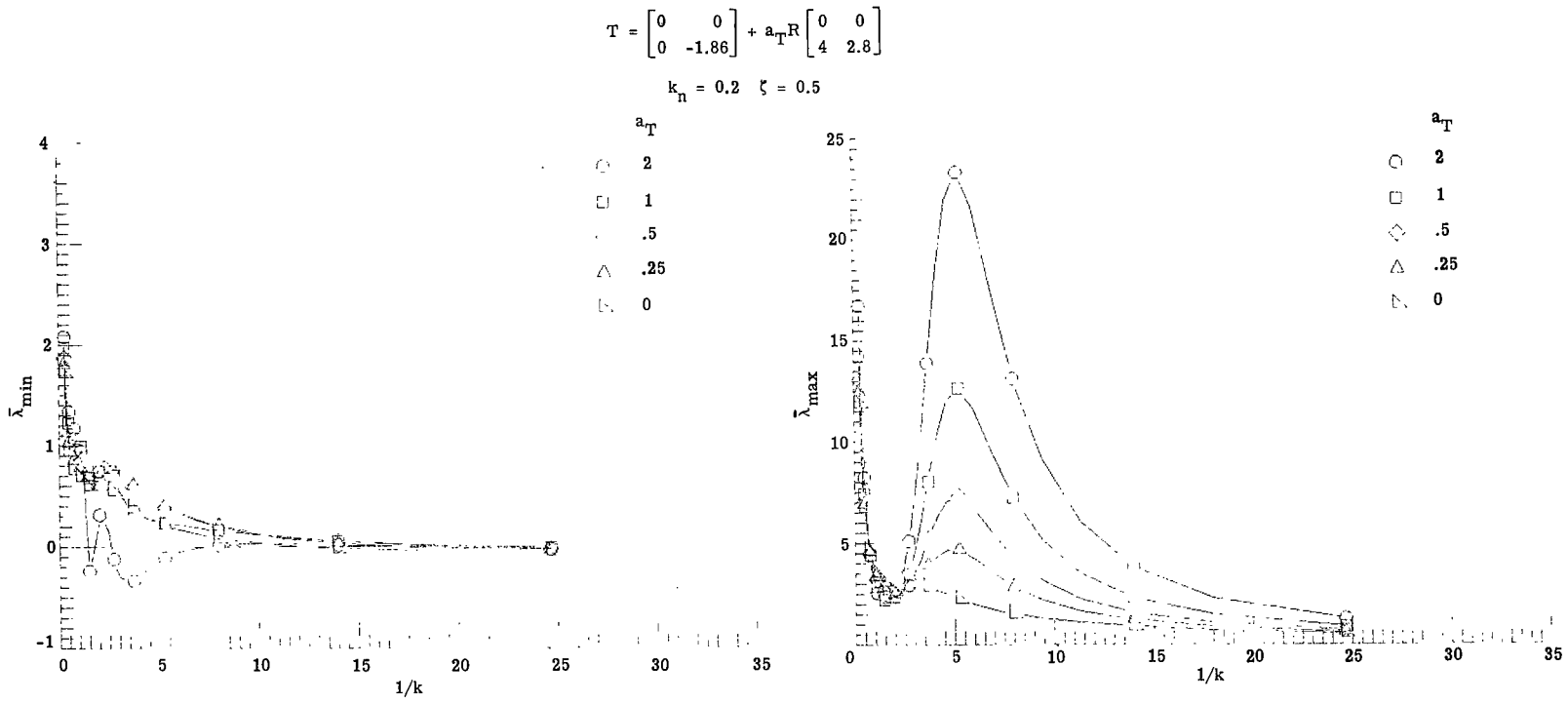

(a) $\bar{\lambda}_{min}$.

(b) $\bar{\lambda}_{max}$.

Figure 19.- Variation of $\bar{\lambda}$ with 1/k at M = 0.9 for different scaled ranges of $|G_{ij}|$. Trailing-edge control system using localized damping type transfer function.

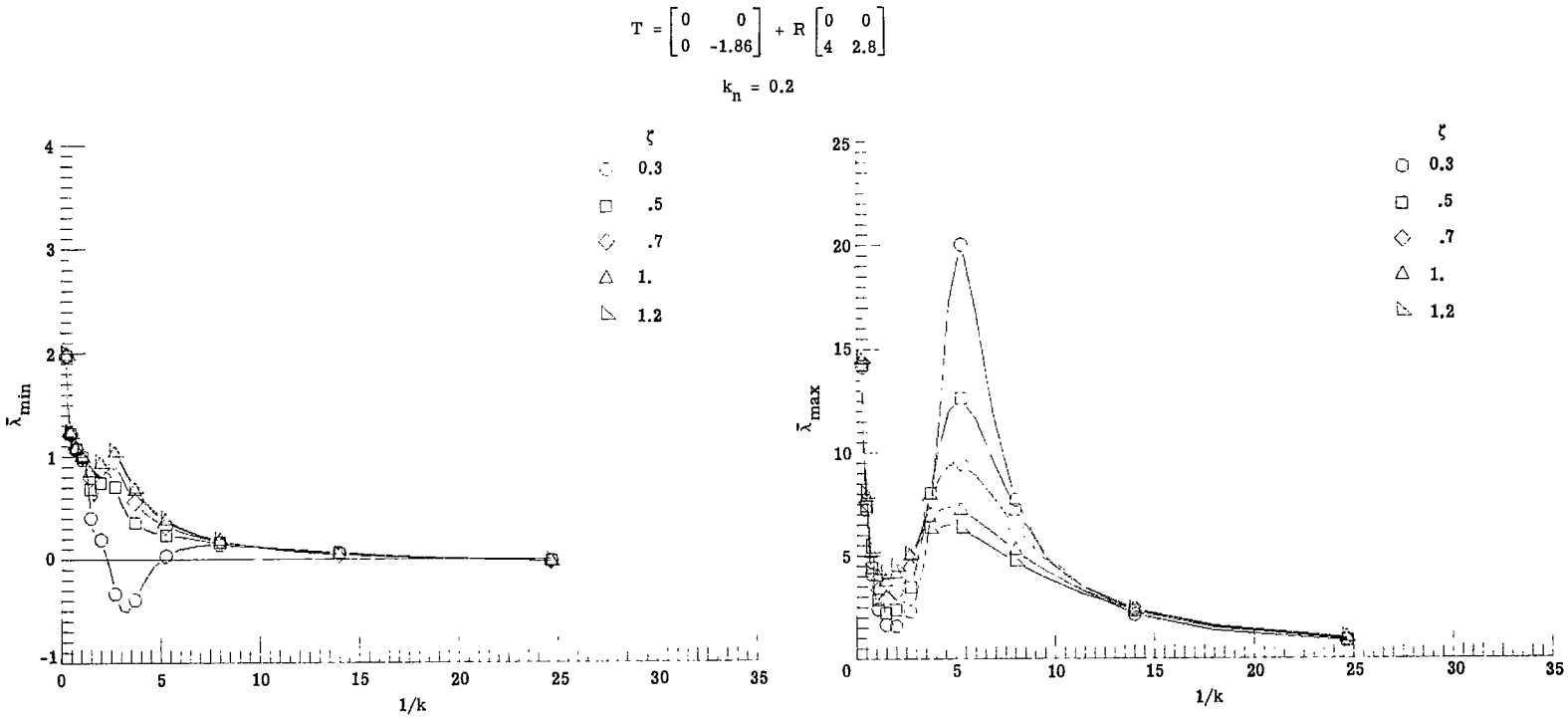

(a) $\bar{\lambda}_{min}$.

(b) $\bar{\lambda}_{max}$.

Figure 20.- Variation of $\bar{\lambda}$ with 1/k at M = 0.9 for different values of ζ. Trailing-edge control system using localized damping type transfer function.

$$T = \begin{bmatrix} 0 & 0 \\ 0 & -1.86 \end{bmatrix} + R \begin{bmatrix} 0 & 0 \\ 4 & 2.8 \end{bmatrix}$$

$\zeta = 0.5$

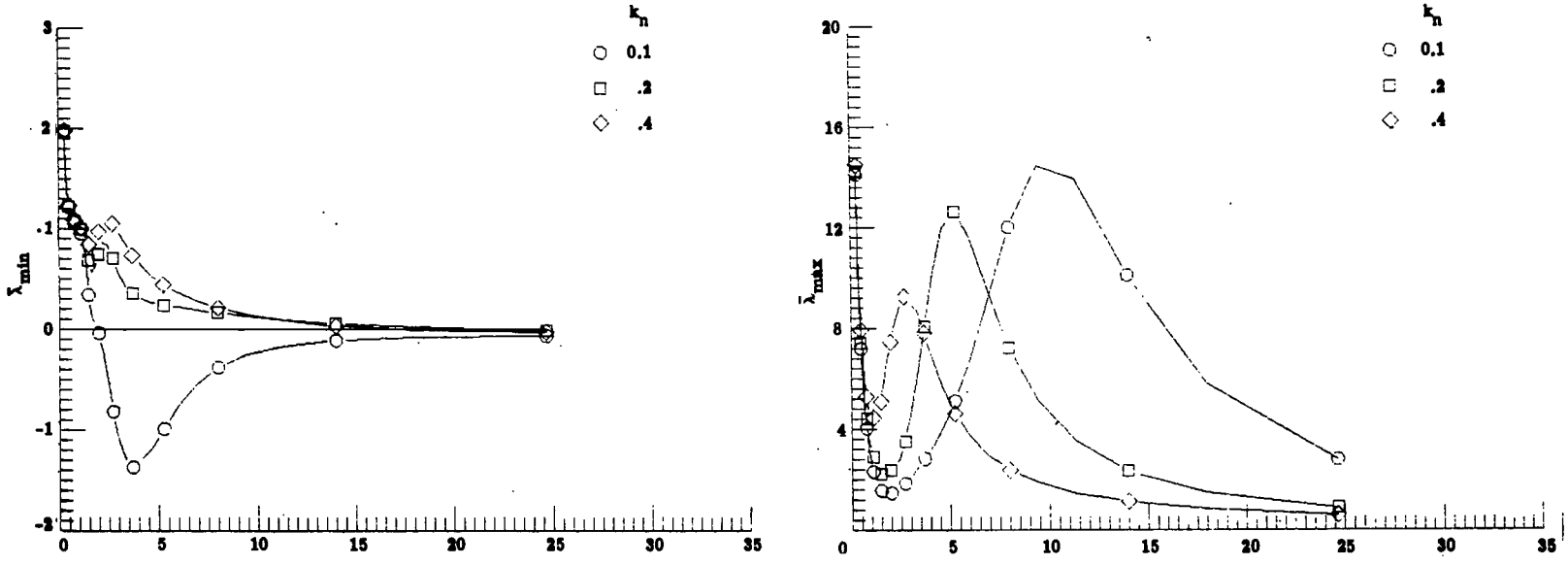

(a) $\bar{\lambda}_{min}$.

(b) $\bar{\lambda}_{max}$.

Figure 21.- Variation of $\bar{\lambda}$ with $1/k$ at $M = 0.9$ for different values of k_n. Trailing-edge control system using localized damping type transfer function.

$$T = \begin{bmatrix} 0 & 0 \\ 0 & -1.86 \end{bmatrix} + R \begin{bmatrix} -4 & 4 \\ 4 & 2.8 \end{bmatrix}$$

$k_n = 0.2 \quad \zeta = 0.5$

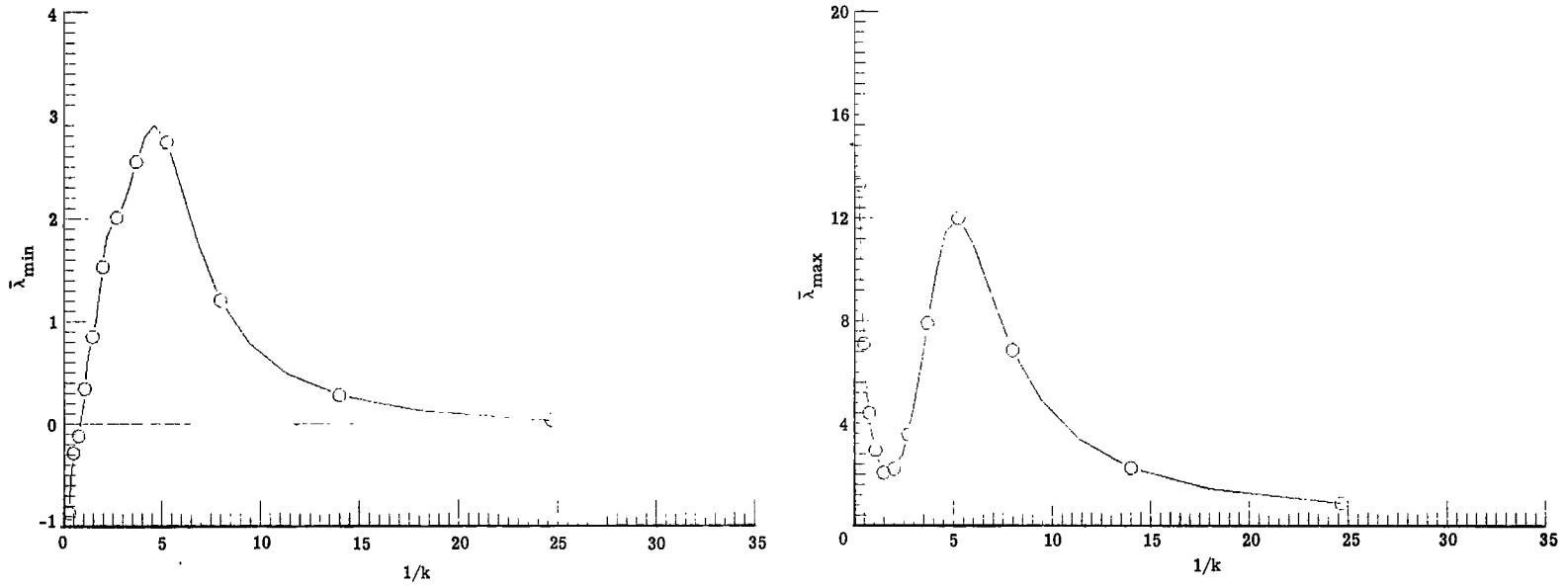

(a) $\bar{\lambda}_{min}$.

(b) $\bar{\lambda}_{max}$.

Figure 22.- Optimum variation of $\bar{\lambda}$ with $1/k$ for a leading-edge—trailing-edge control system (with $G_{21} = 4$) using localized damping type transfer function.

$$T = \begin{bmatrix} 0 & 0 \\ 0 & -1.86 \end{bmatrix} + R \begin{bmatrix} -4 & 4 \\ 4 & 2.8 \end{bmatrix}$$

$k_n = 0.2 \quad \zeta = 0.5$

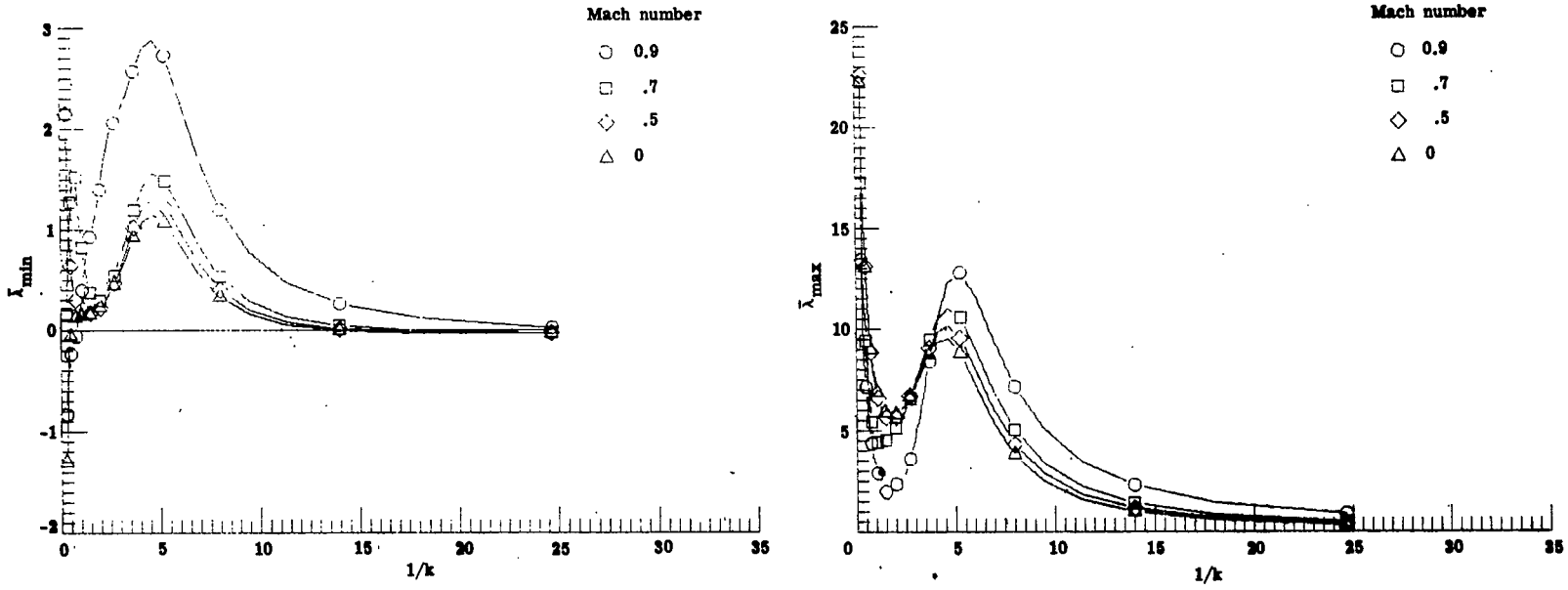

(a) $\bar{\lambda}_{min}$.

(b) $\bar{\lambda}_{max}$.

Figure 23.- Variation of $\bar{\lambda}$ with 1/k at different Mach numbers. Leading-edge—trailing-edge control system using localized damping type transfer function.

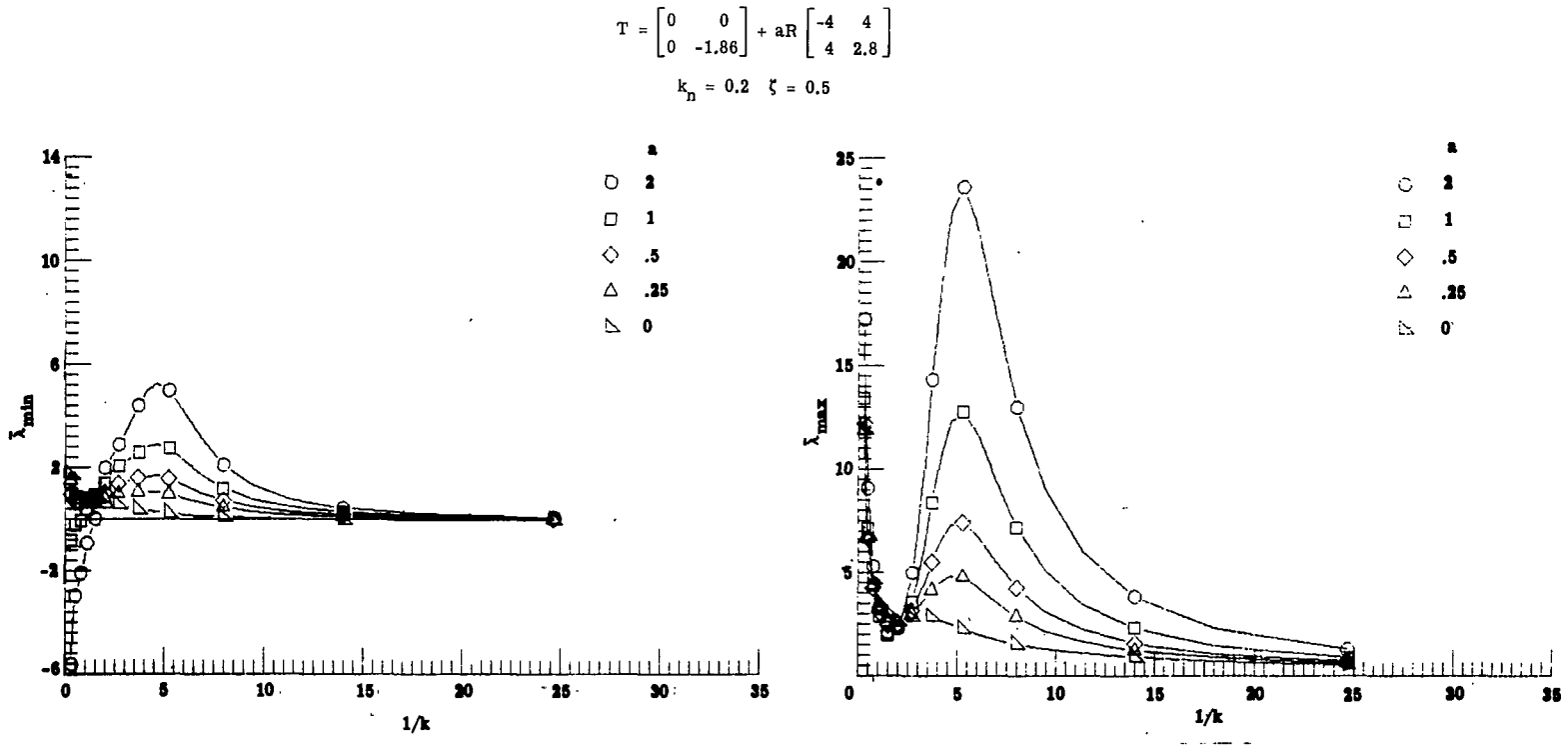

(a) $\bar{\lambda}_{min}$.

(b) $\bar{\lambda}_{max}$.

Figure 24.- Variation of $\bar{\lambda}$ with 1/k at M = 0.9 for different scaled ranges of $|G_{ij}|$. Leading-edge—trailing-edge control system using localized damping type transfer function.

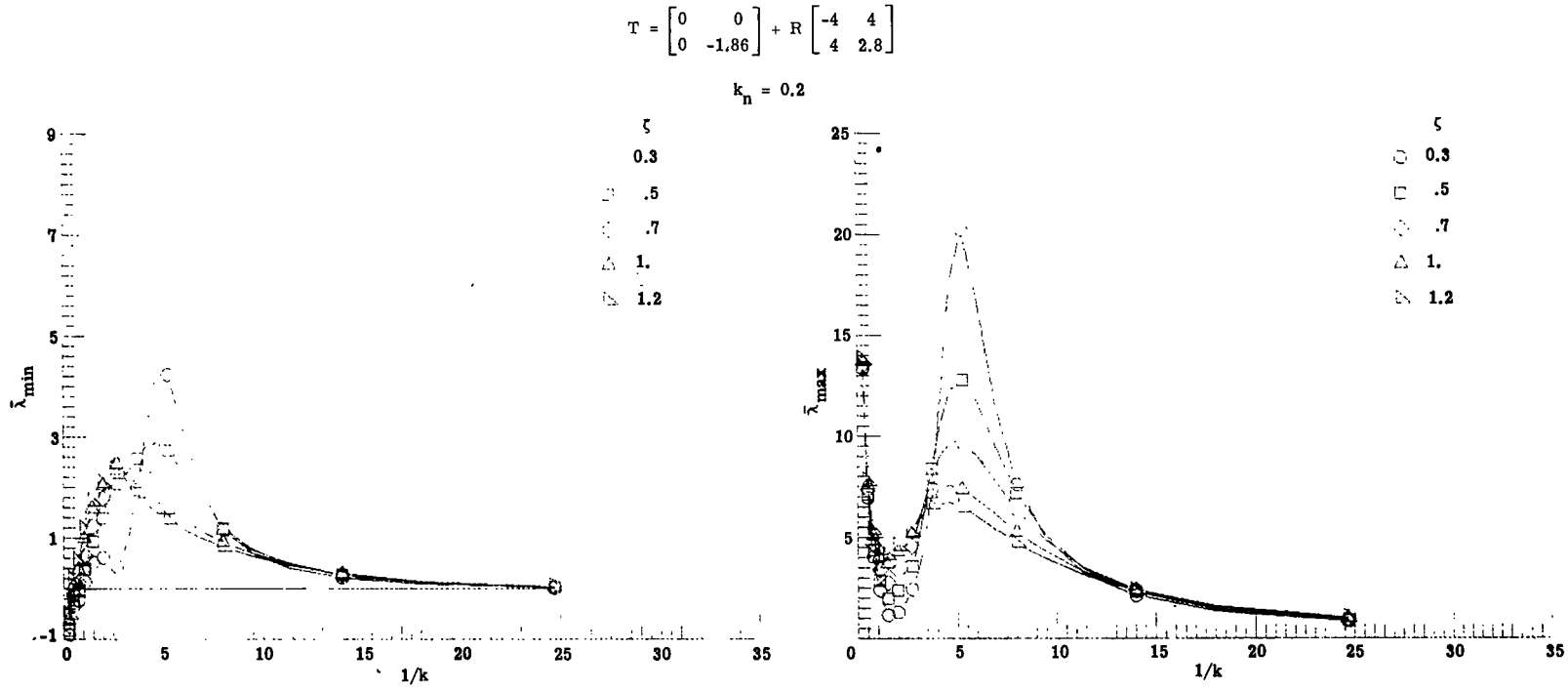

(a) $\bar{\lambda}_{min}$.

(b) $\bar{\lambda}_{max}$.

Figure 25.- Variation of $\bar{\lambda}$ with 1/k at M = 0.9 for different values of ζ. Leading-edge—trailing-edge control system using localized damping type transfer function.

$$T = \begin{bmatrix} 0 & 0 \\ 0 & -1.86 \end{bmatrix} + R \begin{bmatrix} -4 & 4 \\ 4 & 2.8 \end{bmatrix}$$

$\zeta = 0.5$

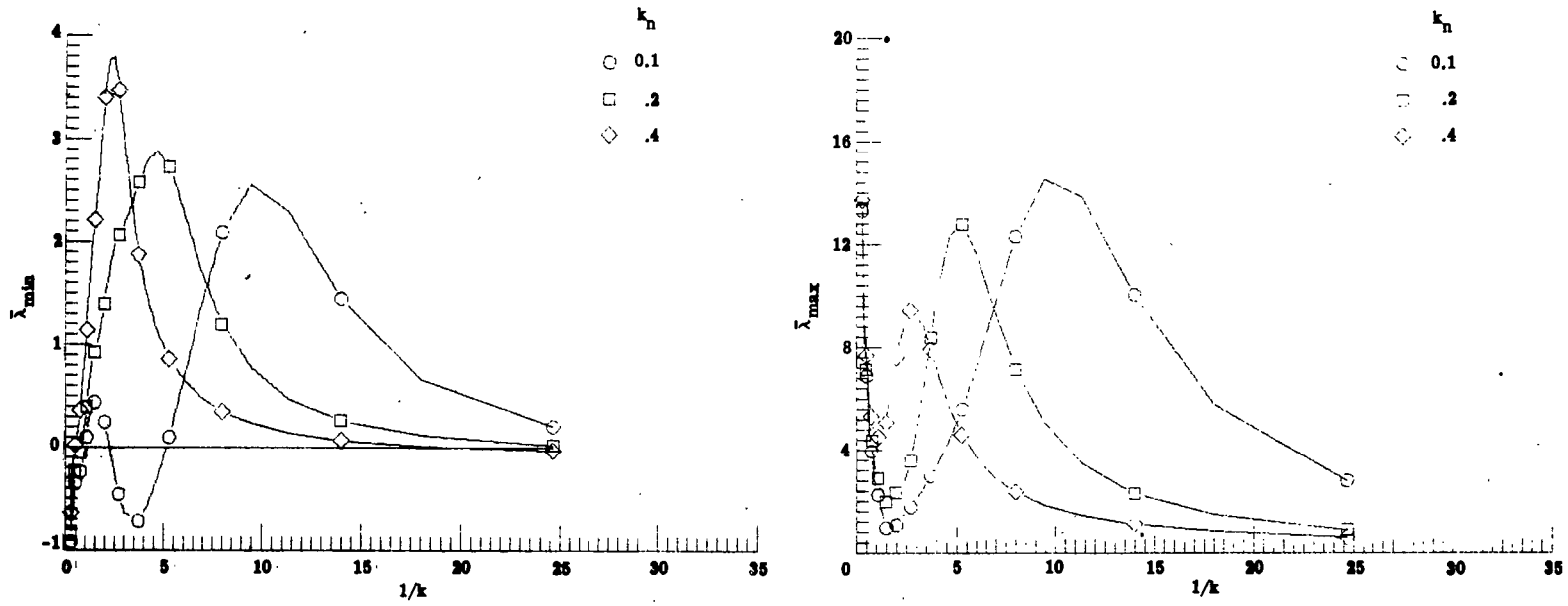

(a) $\bar{\lambda}_{min}$.

(b) $\bar{\lambda}_{max}$.

Figure 26.- Variation of $\bar{\lambda}$ with 1/k at M = 0.9 for different values of k_n. Leading-edge—trailing-edge control system using localized damping type transfer function.

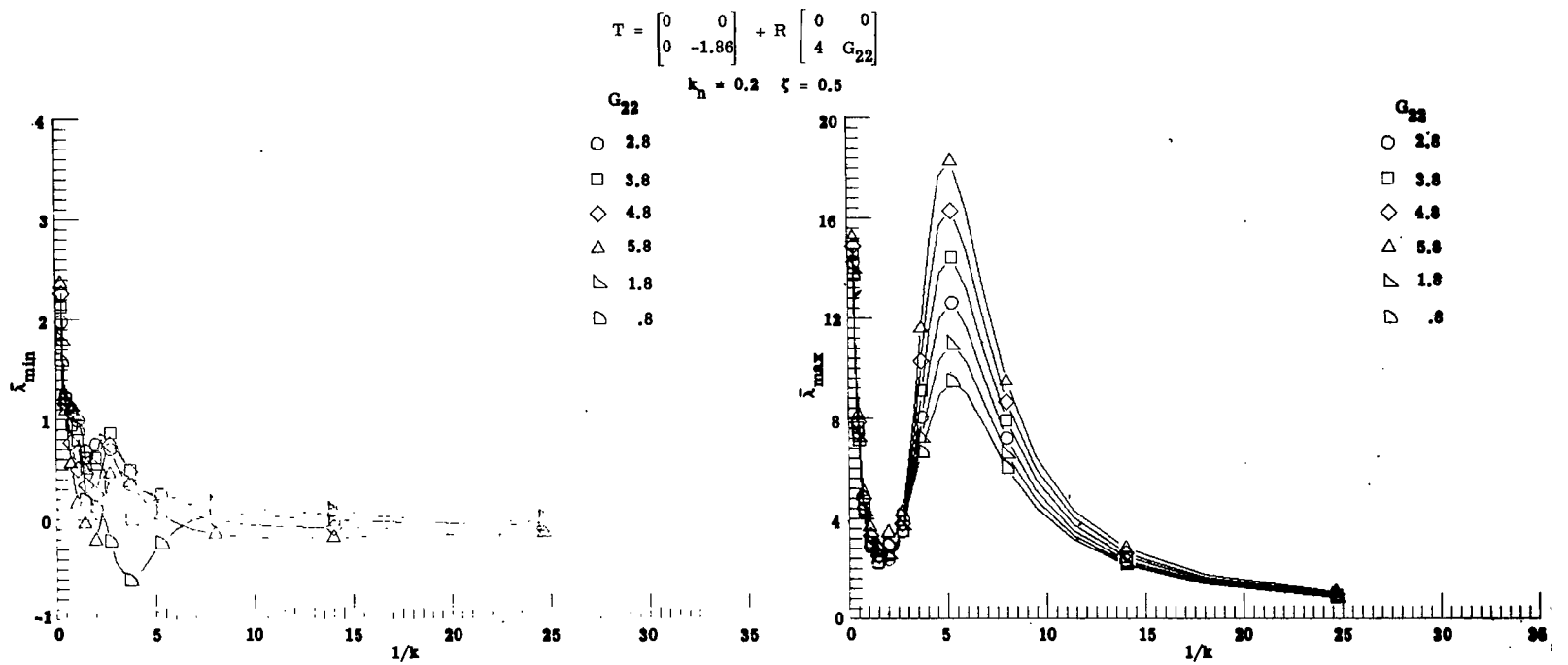

(a) $\bar{\lambda}_{min}$.

(b) $\bar{\lambda}_{max}$.

Figure 27.- Effects on $\bar{\lambda}$ of variation of G_{22} around its optimum value. Trailing-edge control system at $M = 0.9$ using localized damping type transfer function.

4 1 090277 S00903DS
DEPT OF THE AIR FORCE
AF WEAPONS LABORATORY
ATTN: TECHNICAL LIBRARY (SUL)
KIRTLAND AFB NM 87117

"The aer... United States shall be conducted so as to contribute . . . to the expansion of human knowledge of phenomena in the atmosphere and space. The Administration shall provide for the widest practicable and appropriate dissemination of information concerning its activities and the results thereof."

—NATIONAL AERONAUTICS AND SPACE ACT OF 1958

NASA SCIENTIFIC AND TECHNICAL PUBLICATIONS

TECHNICAL REPORTS: Scientific and technical information considered important, complete, and a lasting contribution to existing knowledge.

TECHNICAL NOTES: Information less broad in scope but nevertheless of importance as a contribution to existing knowledge.

TECHNICAL MEMORANDUMS: Information receiving limited distribution because of preliminary data, security classification, or other reasons. Also includes conference proceedings with either limited or unlimited distribution.

CONTRACTOR REPORTS: Scientific and technical information generated under a NASA contract or grant and considered an important contribution to existing knowledge.

TECHNICAL TRANSLATIONS: Information published in a foreign language considered to merit NASA distribution in English.

SPECIAL PUBLICATIONS: Information derived from or of value to NASA activities. Publications include final reports of major projects, monographs, data compilations, handbooks, sourcebooks, and special bibliographies.

TECHNOLOGY UTILIZATION PUBLICATIONS: Information on technology used by NASA that may be of particular interest in commercial and other non-aerospace applications. Publications include Tech Briefs, Technology Utilization Reports and Technology Surveys.

Details on the availability of these publications may be obtained from:

SCIENTIFIC AND TECHNICAL INFORMATION OFFICE

NATIONAL AERONAUTICS AND SPACE ADMINISTRATION

Washington, D.C. 20546